Stationary and slowly moving localised pulses in a singularly perturbed Brusselator model

J. C. TZOU, A. BAYLISS, B. J. MATKOWSKY and V. A. VOLPERT

*Department of Engineering Sciences and Applied Mathematics, Northwestern University,
Evanston, IL 60208-3125, USA*
email: b-matkowsky@northwestern.edu

Recent attention has focused on deriving localised pulse solutions to various systems of reaction–diffusion equations. In this paper, we consider the evolution of localised pulses in the Brusselator activator–inhibitor model, long considered a paradigm for the study of non-linear equations, in a finite one-dimensional domain with feed of the inhibitor through the boundary and global feed of the activator. We employ the method of matched asymptotic expansions in the limit of small activator diffusivity and small activator and inhibitor feeds. The disparity of diffusion lengths between the activator and inhibitor leads to pulse-type solutions in which the activator is localised while the inhibitor varies on an $O(1)$ length scale. In the asymptotic limit considered, the pulses become spikes described by Dirac delta functions and evolve slowly in time until equilibrium is reached. Such quasi-equilibrium solutions with N activator pulses are constructed and a differential-algebraic system of equations (DAE) is derived, characterising the slow evolution of the locations and the amplitudes of the pulses. We find excellent agreement for the pulse evolution between the asymptotic theory and the results of numerical computations. An algebraic system for the equilibrium pulse amplitudes and locations is derived from the equilibrium points of the DAE system. Both symmetric equilibria, corresponding to a common pulse amplitude, and asymmetric pulse equilibria, for which the pulse amplitudes are different, are constructed. We find that for a positive boundary feed rate, pulse spacing of symmetric equilibria is no longer uniform, and that for sufficiently large boundary flux, pulses at the edges of the pattern may collide with and remain fixed at the boundary. Lastly, stability of the equilibrium solutions is analysed through linearisation of the DAE, which, in contrast to previous approaches, provides a quick way to calculate the small eigenvalues governing weak translation-type instabilities of equilibrium pulse patterns.

Key words: Brusselator model; Pulse evolution; Quasi-equilibria; Differential-algebraic equations; Matched asymptotic expansions; Singular perturbations

1 Introduction

Since Turing [27] showed that diffusion-driven instabilities of a spatially homogeneous steady state could give rise to spatially complex patterns in a mixture of chemically reacting species, reaction–diffusion equations have been paradigms of spatio-temporal pattern formation. Much of the analysis since has been weakly non-linear, involving small amplitude patterns arising from small perturbations of the unstable uniform steady state. However, numerical studies (see, e.g. [25] for numerical simulations of the

two-dimensional Gray–Scott model) have shown that large-amplitude perturbations can lead to the formation of localised structures, solutions far from equilibrium and thus not amenable to weakly non-linear analysis. Instead, the method of matched asymptotic expansions has been applied to construct such localised solutions. Early works involving the one-dimensional Gray–Scott model on the infinite line include Doelman *et al.* [3–5], where a dynamical systems approach was taken to construct localised pulse solutions and study their stability by analysing a non-linear eigenvalue problem. In [21], stability analysis of a one-dimensional pulse to transverse perturbations in the second dimension was performed. Extensions of these results to incorporate finite domain effects for models, such as the Gray–Scott (e.g. [1, 17]), Gierer–Meinhardt (e.g. [10, 11]) and Schnakenberg (e.g. [19, 30]) models, have been of recent interest. In one dimension, behaviours such as slow pulse evolution, pulse splitting, and pulse oscillations, have been predicted analytically and confirmed numerically. In this work, we consider the slow evolution of pulses in the one-dimensional activator–inhibitor Brusselator model (see, e.g. [28] and references therein), long a paradigm of non-linear analysis.

The Brusselator model describes the space–time dependence of the concentrations of the intermediate products U (the activator) and V (the inhibitor) in the sequence of reactions

$$E \rightarrow U, \quad B + U \rightarrow V + P, \quad 2U + V \rightarrow 3U, \quad U \rightarrow Q. \tag{1.1}$$
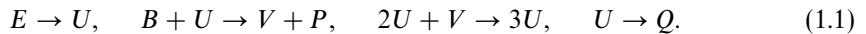
The global reaction is $E + B \rightarrow P + Q$, corresponding to the transformation of reactants E and B into products P and Q. The third reaction of sequence (1.1) is autocatalytic in that U drives its own production; thus, U is the activator. The autocatalytic reaction requires the presence of V to proceed; the depletion of V in the autocatalytic process acts as an inhibition mechanism to limit the growth of U. Thus, V is the inhibitor and is subject to low concentrations in regions of high activator concentration. A different scenario is seen in the Gierer–Meinhardt model [8] where the autocatalytic reaction is impeded by the presence of an inhibitor. In this case, high concentrations of the inhibitor are observed in regions of high activator concentration.

Due to the third reaction in (1.1), the Brusselator model shares the same cubic non-linearity as the Gray–Scott and Schnakenberg models but differs in that the former contains a global feed term of the activator and not of the inhibitor. The feed of the activator comes from the first reaction in (1.1). The result of a global activator feed term is that localised pulses in the concentration of the activator can decay to either a zero or non-zero value away from their centres, depending on the value of the feed term. We find that the absence or presence of the activator feed term has an important role in the evolution of the pulses. This is in contrast to the Gray–Scott and Schnakenberg models, where pulses always decay to zero away from their centres. Further, while many previous studies considered pure Neumann boundary conditions for both the activator and inhibitor, we allow for the possibility of a boundary feed term of the inhibitor, which we find alters the equilibrium solutions as well as the interaction between pulses and boundaries.

In [22], localised solutions were computed numerically and analysed for a variation of the conventional Brusselator model. Instead of the concentration of the reactant E being kept constant as is the case in most studies of the Brusselator model, it was allowed to vary with space and time. The diffusion rate of E was also taken to be significantly larger

than those of U and V. Localised structures exhibited by the conventional Brusselator model near a co-dimension two point were numerically observed under periodic [26] and, additionally, pure Neumann [2] boundary conditions with similar diffusivities of the activator and inhibitor. In the following analysis, we consider a singular perturbation of the conventional Brusselator model with an asymptotically small activator–inhibitor diffusivity ratio, leading to the formation of localised pulses in the concentration of the activator. Assuming (without loss of generality) that all rate constants of the reactions in (1.1) are unity, the conventional dimensionless Brusselator model in a one-dimensional domain with slow diffusion of the activator and constant influx of the inhibitor from the boundaries can be written as

$$u_t = \epsilon^2 u_{xx} + \mathscr{E} - (B+1)u + vu^2, \qquad -1 < x < 1, \qquad u_x(\pm 1, t) = 0, \qquad t > 0, \qquad (1.2a)$$

$$v_t = D v_{xx} + Bu - vu^2, \qquad -1 < x < 1, \qquad v_x(\pm 1, t) = \pm \mathscr{A}, \qquad t > 0, \qquad (1.2b)$$

supplemented by appropriate initial conditions, where $u \geqslant 0$ is the activator concentration (which will be seen to be the localised variable), $v \geqslant 0$ is the inhibitor, $0 < \epsilon \ll 1$, and $\mathscr{A}$, B, D and $\mathscr{E}$ are non-negative constants. In a study of mesa-type patterns, Kolokolnikov *et al.* [15] consider a slightly different form in which the first and last steps of (1.1) occur much more slowly than the other reactions, leading to the kinetic terms of (1.2a) being $r\mathscr{E} - (B+r)u + vu^2$ with r small.

The activator drives its own reaction through a positive feedback (the vu^2 term in (1.2a)), while its growth is controlled by the inhibitor, for which there is negative feedback, represented by the $-vu^2$ term in (1.2b) (see [14]). The condition that the inhibitor diffuses significantly faster than the activator ($D \gg \epsilon^2$) is essential for the formation of pulses, as in [20]. Indeed, the self-production of the activator in a region of length $O(\epsilon)$ cannot be sufficiently suppressed by the inhibitor as the strong inflow of the inhibitor from the peripheral regions continues to feed the production of the activator (see [13, 14]). It is for this reason, along with the slow diffusion of the activator, that we expect the formation of localised pulses in the activator, while the inhibitor varies over an $O(1)$ length scale. As a result, the leading order interaction between pulses is due to the slow spatial variation of the inhibitor variable, this interaction having thus been termed semi-strong [6]. This regime is in contrast to the weak interaction regime, in which $D = O(\epsilon^2)$, $\epsilon \ll 1$ and studied in [23] and [24] for the Gray–Scott model, yielding both pulse-splitting behaviour and pulse collisions. In this latter regime, both the activator and the inhibitor are localised, hence the weaker pulse interaction.

As mentioned, pulse patterns in reaction–diffusion models in one dimension (e.g. [11, 17, 30]) have previously been considered with no-flux boundary conditions, leading to repulsive pulse–boundary interactions. In contrast, we will show that, in this Brusselator model with boundary flux, the boundaries of the domain can be attracting for large enough boundary flux. We begin in Section 3 by using matched asymptotic expansions to derive a system of differential-algebraic equations (DAE) describing the slow evolution of N-pulse quasi-equilibrium patterns (see [7] for a treatment of slow pulse evolution in a regularised Gierer–Meinhardt model). Considering special two and three-pulse cases, we demonstrate that pulses at the edges of the pulse pattern (edge pulses) can be captured by the boundary when the boundary feed increases such that their equilibrium positions no longer lie inside

the domain. The term 'capture' herein will refer to the event in which a pulse collides with and remains fixed at the boundary and, in the cases that we considered, its amplitude changes dramatically over a relatively short time. The presence of boundary flux also affects equilibrium pulse spacing and requires modification of the 'gluing' construction for equilibrium pulse patterns employed in [18] and [29] for the Gray–Scott and Gierer–Meinhardt models. Instead, in Section 4, we construct equilibrium solutions by deriving an algebraic system for equilibrium pulse amplitudes and locations from equilibrium points of the DAE. As in the aforementioned studies, symmetric equilibria, corresponding to a common pulse amplitude, and asymmetric pulse equilibria, for which pulse amplitudes are different, are found. For symmetric equilibria, we show that pulse spacing is non-uniform due to boundary flux, and we also give a general criterion for edge pulses to be captured by the boundary. Finally, in Section 5, the stability of the equilibrium points of DAE dynamics is calculated analytically, which, in contrast to the approach in [18] and [29] for Gray–Scott and Gierer–Meinhardt models, provides a quick way to calculate the small eigenvalues governing the weak translation-type instabilities of pulse patterns. In this paper, however, no analysis of $O(1)$ time-scale fast instabilities of the pulse profile, typically governed by a non-local eigenvalue problem (see, e.g. [16, 30]), is carried out.

2 Scalings

To motivate the scalings with respect to ϵ of the parameters and variables in (1.2), we first note that u is the localised variable for which the inner region of each pulse has $O(\epsilon)$ width. We also assume that, since v is the slowly varying global variable, it is of the same order in both the inner region and the outer region away from each pulse. Thus, in order to balance v_x to the boundary feed rate term $\mathscr{A}$ in (1.2b), $v = O(\mathscr{A})$ in all regions. In the inner region, we let $u = O(U_{in})$ and assume that $U_{in} \gg \mathscr{E}$. In order for the cubic term in (1.2a) to balance the derivative and linear terms and yield a homoclinic solution in u, we require that $U_{in}\mathscr{A} = O(1)$, or $U_{in} = O(\mathscr{A}^{-1})$. In the outer region, the term vu^2 in (1.2b) as $\epsilon \to 0$ can be represented as a delta sequence with weight $O(\epsilon U_{in}^2 \mathscr{A})$, which must balance the v_{xx} term, yielding $\mathscr{A} = O(\epsilon U_{in}^2 \mathscr{A})$. Thus, $U_{in} = O(\epsilon^{-1/2})$ and $\mathscr{A} = O(\epsilon^{1/2})$. The same scaling is obtained from repeating this argument for the Bu term in (1.2b) with $B = O(1)$. Finally, from (1.2a), assuming $vu^2 \ll u$, we have $u = O(U_{out}) = O(\mathscr{E})$ in the outer region, which must balance the v_{xx} term in (1.2b) so that $\mathscr{E} = O(\epsilon^{1/2})$. Thus, $u = O(\epsilon^{-1/2})$ in the inner region while $u = O(\epsilon^{1/2})$ in the outer region. Globally, $v = O(\epsilon^{1/2})$. With these scalings for $\mathscr{A}$ and $\mathscr{E}$, we rewrite (1.2) as

$$u_t = \epsilon^2 u_{xx} + \epsilon^{1/2}E - (B+1)u + vu^2, \qquad -1 < x < 1, \qquad u_x(\pm 1, t) = 0, \qquad t > 0, \quad (2.1a)$$

$$v_t = Dv_{xx} + Bu - vu^2, \qquad -1 < x < 1, \qquad v_x(\pm 1, t) = \pm\epsilon^{1/2}A, \qquad t > 0. \qquad (2.1b)$$

All subsequent analysis and computations will be performed on this system.

3 Evolution of multiple pulses

Using matched asymptotic expansions, we now construct an N-pulse quasi-equilibrium solution to (2.1) that evolves on an asymptotically slow time scale $T = \epsilon^2 t$; the scale

determined by enforcing consistency in the solvability condition in the inner problem. Assuming an $O(1)$ separation distance between adjacent pulses and between edge pulses and the boundaries, we separately consider the inner problem for each individual pulse j. That is, in the jth inner region, we recall the inner scalings in Section 2 and introduce the inner variables

$$u \sim \frac{1}{\epsilon^{1/2}} U_j(y_j) = \frac{1}{\epsilon^{1/2}}(U_{j_0} + \epsilon U_{j_1} + \dots), \qquad v \sim \epsilon^{1/2} V_j(y_j) = \epsilon^{1/2}(V_{j_0} + \epsilon V_{j_1} + \dots);$$

$$y_j = \frac{x - x_j(T)}{\epsilon}, \tag{3.1}$$

where we assume $x_i < x_j$ for $i < j$. The solution is thus characterised by N pulses whose form remains constant while their centre and amplitude may vary on a slow time scale. Substituting (3.1) into (2.1), we find the leading order equations for U_{j_0} and V_{j_0}:

$$U_{j_0}'' - (B+1)U_{j_0} + V_{j_0} U_{j_0}^2 = 0, \qquad -\infty < y_j < \infty, \tag{3.2a}$$

$$U_{j_0} \to 0 \quad \text{as} \quad |y_j| \to \infty, \tag{3.2b}$$

and

$$D V_{j_0}'' = 0, \qquad -\infty < y_j < \infty, \tag{3.3a}$$

$$V_{j_0} \quad \text{bounded as} \quad |y_j| \to \infty, \tag{3.3b}$$

where the decay condition on U_{j_0} at $\pm\infty$ and the boundedness condition on V_{j_0} are required to match to the outer solution. We remove the translational invariance of (3.2) by requiring that $U_{j_0}'(0) = 0$. Here, the primes indicate differentiation with respect to y_j. Since (3.3) leads to V_{j_0} being a constant, the leading order inner equations are uncoupled. We can then readily solve (3.2) and (3.3) as

$$V_{j_0} = \bar{V}_j(x_1, \dots, x_N) \equiv \bar{V}_j, \qquad j = 1, \dots, N,$$

and

$$U_{j_0}(y_j) = \frac{3(B+1)}{2\bar{V}_j} \operatorname{sech}^2\left(\frac{\sqrt{B+1}}{2} y_j\right), \tag{3.4}$$

where $\bar{V}_j$ is spatially independent but can depend on $x_1, \dots, x_N$. We refer to the pre-factor in (3.4) as the pulse amplitude, which is inversely proportional to $\bar{V}_j$. We will see below that, like x_j, $\bar{V}_j$ evolves on an $O(\epsilon^2)$ time scale. At the next order, we obtain for U_{j_1} and V_{j_1}

$$U_{j_1}'' - (B+1)U_{j_1} + 2\bar{V}_j U_{j_0} U_{j_1} = -x_j'(T)U_{j_0}' - V_{j_1} U_{j_0}^2 - E, \qquad -\infty < y_j < \infty, \tag{3.5a}$$

$$U_{j_1} \to \frac{E}{B+1} \quad \text{as} \quad |y_j| \to \infty, \tag{3.5b}$$

and

$$D V_{j_1} = V_{j_0} U_{j_0}^2 - B U_{j_0}, \qquad -\infty < y_j < \infty. \tag{3.6}$$

The limiting condition (3.5b) follows from the fact that in the outer region $u \sim \epsilon^{1/2}E/(B+1)$, which can be deduced from applying the outer region scaling $u = O(\epsilon^{1/2}) = v$

and solving for u in (2.1a). In the far field, we allow V_{j_1} to grow linearly in y_j, with the precise conditions to come from matching to the outer solution. The solution to (3.6) can then be readily obtained, which we write as

$$V_{j_1}(y) = -\frac{3(B+1)}{2D\bar{V}_j}\text{sech}^2\left(\frac{\sqrt{B+1}}{2}y_j\right) + \frac{6}{D\bar{V}_j}\log\left(\cosh\left(\frac{\sqrt{B+1}}{2}y_j\right)\right) + c_{j_1}y_j + c_{j_2}, \quad (3.7)$$

where c_{j_1} and c_{j_2}, which may depend on $x_1,\ldots,x_N$, are integration constants. The former determines the linear behaviour of V_{j_1} in the far-field and will be calculated when the inner solution is matched to the outer. Determining c_{j_2} requires higher order matching and is not needed for our purposes.

To use the Fredholm alternative to find an expression for $x_j'(T)$ from (3.5a), we make the substitution $U_{j_1} = W_j + E/(B+1)$ to obtain

$$W_j'' - (B+1)W_j + 2\bar{V}_j U_{j_0} W_j = -2U_{j_0}\bar{V}_j\frac{E}{B+1} - x_j'(T)U_{j_0}' - V_{j_1}U_{j_0}^2, \quad -\infty < y_j < \infty, \tag{3.8a}$$

$$W_j \to 0 \quad \text{as} \quad |y_j| \to \infty. \tag{3.8b}$$

Differentiating (3.2a) with respect to y_j, we find that $W = U_{j_0}'$ is a solution to the homogeneous problem of (3.8a) satisfying (3.8b); thus, the right-hand side of (3.8a) must satisfy the Fredholm condition

$$\int_{-\infty}^{\infty} U_{j_0}'\left(-2U_{j_0}V_{j_0}\frac{E}{B+1} - x_j'(T)U_{j_0}' - V_{j_1}U_{j_0}^2\right)dy_j = 0. \tag{3.9}$$

Noting that V_{j_0} is a constant and that U_{j_0} is an even function (from (3.4)), we use (3.7) to obtain from (3.9)

$$\frac{dx_j}{dT} = \frac{2c_{j_1}}{\bar{V}_j}, \quad j = 1,\ldots,N.$$

Here, c_{j_1}, introduced in (3.7), and $\bar{V}_j$ will be determined by matching the inner solution of v to the outer solution along with a solvability condition. In general, c_{j_1} and $\bar{V}_j$ can depend on x_j, $j = 1,\ldots,N$, resulting in coupling between the N pulses. Since x_j varies slowly in time, so too will $\bar{V}_j$, $j = 1,\ldots,N$, and consequently, the pulse amplitudes.

To solve for v in the outer region, we proceed as in [30] and use the assumption of sufficiently separated pulses to express each term involving u in (2.1b) as a sum of N appropriately weighted delta masses, with each delta mass representing a pulse. With weights equal to the area under each function involving u, we approximate the Bu term in (2.1b) as

$$Bu \sim \epsilon^{1/2}\frac{BE}{B+1} + \sum_{j=1}^{N} w_{j_1}\delta(x - x_j); \quad w_{j_1} = \epsilon^{1/2}\int_{-\infty}^{\infty} U_{j_0}\,dy_j = \epsilon^{1/2}\frac{6B\sqrt{B+1}}{\bar{V}_j}, \quad (3.10)$$

and the vu^2 term in (2.1b) as

$$vu^2 \sim \sum_{j=1}^{N} w_{j_2}\delta(x - x_j); \quad w_{j_2} = \epsilon^{1/2}\int_{-\infty}^{\infty} V_{j_0}U_{j_0}^2\,dy_j = \epsilon^{1/2}\frac{6(B+1)^{3/2}}{\bar{V}_j}. \tag{3.11}$$

Then, using (3.10) and (3.11) in (2.1b), and re-scaling $v = \epsilon^{1/2}v$, we find that, to leading order, v satisfies

$$Dv_{xx} + \frac{BE}{B+1} - 6\sqrt{B+1}\sum_{j=1}^{N}\frac{1}{\bar{V}_j}\delta(x-x_j) = 0, \quad -1 < x < 1, \quad v_x(\pm 1) = \pm A. \quad (3.12)$$

Integrating (3.12) over $-1 < x < 1$ and applying the boundary conditions on v_x, we find that $\bar{V}_j$ must satisfy the solvability condition

$$\sum_{j=1}^{N}\frac{1}{\bar{V}_j} = \frac{AD + F}{3\sqrt{B+1}}, \quad (3.13)$$

where

$$F \equiv \frac{BE}{B+1}. \quad (3.14)$$

With the constraint (3.13), we solve for $v(x)$ up to an arbitrary constant $\bar{v}$ in terms of a modified Green's function $G(x; x_j)$,

$$v = \bar{v} + \frac{A}{2}x^2 + 6\sqrt{B+1}\sum_{j=1}^{N}\frac{1}{\bar{V}_j}G(x; x_j), \quad (3.15)$$

where $G(x; x_j)$ satisfies

$$DG_{xx}(x; x_j) + \frac{1}{2} = \delta(x-x_j), \quad -1 < x < 1, \quad G_x(\pm 1; x_j) = 0, \quad \int_{-1}^{1}G(x; x_j)\,dx = 0, \quad (3.16)$$

with uniqueness achieved through the constraint in (3.16). The solution to (3.16) is

$$G(x; x_j) = -\frac{1}{4D}(x^2 + x_j^2) + \frac{1}{2D}|x - x_j| - \frac{1}{6D}.$$

Now to determine $\bar{v}$ and c_{i_1}, we match the behaviour of v and V_i near x_i for $i = 1,\ldots,N$. Expanding $v(x)$ in (3.15) in powers of $(x - x_i)$ as $x \to x_i^+$, we find

$$v \sim \bar{v} + \frac{A}{2}x_i^2 + 6\sqrt{B+1}\sum_{j=1}^{N}\frac{1}{\bar{V}_j}G(x_i; x_j) + \left(Ax_i + 6\sqrt{B+1}\sum_{j=1}^{N}\frac{1}{\bar{V}_j}G_x(x_i^+; x_j)\right)(x - x_i), \quad (3.17)$$

which must match the behaviour of V_i as $y_i \to \infty$:

$$V_i \sim \bar{V}_i + \epsilon\left(\frac{3\sqrt{B+1}}{D\bar{V}_i}y_j + c_{i_1}y_j + c_{i_2} - \log 2\right). \quad (3.18)$$

Matching the appropriate terms in (3.17) and (3.18) while recalling that $y_i = (x - x_i)/\epsilon$, we find that

$$\bar{v} = \bar{V}_i - \frac{A}{2}x_i^2 - 6\sqrt{B+1}\sum_{j=1}^{N}\frac{1}{\bar{V}_j}G(x_i; x_j),$$

and

$$c_{i_1} = -\frac{3\sqrt{B+1}}{D\bar{V}_i} + Ax_i + 6\sqrt{B+1}\sum_{j=1}^{N}\frac{1}{\bar{V}_j}G_x(x_i^+;x_j), \qquad (3.19)$$

where $\bar{v}$ is independent of i. Matching the behaviours of v and V_i as $x \to x_i^-$ and $y_i \to -\infty$, respectively, yields the equivalent expression

$$c_{i_1} = \frac{3\sqrt{B+1}}{D\bar{V}_i} + Ax_i + 6\sqrt{B+1}\sum_{j=1}^{N}\frac{1}{\bar{V}_j}G_x(x_i^-;x_j). \qquad (3.20)$$

We now summarise the results for an N-pulse quasi-equilibrium solution to (2.1) in the following result.

Principal Result I *Let $\epsilon \to 0$ in (2.1) and assume $O(1)$ separation between adjacent pulses as well as $O(1)$ separation between edge pulses and nearest boundaries. Then, the leading order quasi-equilibrium N-pulse solutions for u and v are given by*

$$u(x) \sim \frac{1}{\epsilon^{1/2}}\left(\sum_{j=1}^{N}\frac{3(B+1)}{2\bar{V}_j}\mathrm{sech}^2\left(\frac{\sqrt{B+1}}{2}\frac{x-x_j}{\epsilon}\right)\right) + \epsilon^{1/2}\left(\frac{E}{B+1} + \sum_{j=1}^{N}W_j\left(\frac{x-x_j}{\epsilon}\right)\right),$$
$$(3.21a)$$

$$v(x) \sim \epsilon^{1/2}\left(\bar{v} + \frac{A}{2}x^2 + 6\sqrt{B+1}\sum_{j=1}^{N}\frac{1}{\bar{V}_j}G(x;x_j)\right), \qquad (3.21b)$$

where W_j is the even solution to (3.8), and $\bar{v}$ and $\bar{V}_j$, $j = 1,\ldots,N$ are determined by the system of $N+1$ equations

$$\bar{v} - \bar{V}_i + 6\sqrt{B+1}\sum_{j=1}^{N}\frac{1}{\bar{V}_j}G(x_i;x_j) = -\frac{A}{2}x_i^2, \quad i = 1,\ldots,N, \qquad (3.22a)$$

$$\sum_{j=1}^{N}\frac{1}{\bar{V}_j} = \frac{AD + \frac{BE}{B+1}}{3\sqrt{B+1}}. \qquad (3.22b)$$

The $O(\epsilon^2)$ time scale evolution of the pulse locations can be computed from

$$\frac{dx_i}{dt} = \epsilon^2\frac{2c_{i_1}}{\bar{V}_i}, \quad i = 1,\ldots,N, \qquad (3.23)$$

where c_{i_1} is computed from (3.19) and $\bar{V}_i$, $i = 1,\ldots,N$ are computed from (3.22). Equations (3.22) and (3.23) with (3.19) form a DAE for the evolution of the pulse locations and $\bar{V}_i$, the inverse proportionality constant of pulse amplitudes, which along with $\bar{v}$, uniquely parameterise a quasi-equilibrium state.

We now consider special cases for which simplifications of the DAE are possible. The simplest is the one-pulse case for which, by (3.22b), $\bar{V}_1$ remains constant for all time. To

leading orders, the solutions u and v are then given by

$$u(x) \sim \frac{1}{\epsilon^{1/2}} \frac{(AD+F)(B+1)}{2} \operatorname{sech}^2 \left(\frac{\sqrt{B+1}}{2} \frac{x-x_1}{\epsilon} \right) + \epsilon^{1/2} \left[\frac{E}{B+1} + W_1 \left(\frac{x-x_1}{\epsilon} \right) \right],$$
(3.24a)

$$v(x) \sim \epsilon^{1/2} \left[-\frac{F}{2D}(x^2 - x_1^2) + \left(A + \frac{F}{D} \right) |x - x_1| + \frac{3\sqrt{B+1}}{AD+F} \right],$$
(3.24b)

while the centre of the pulse evolves on a slow time scale as

$$x_1(t) = x_1(0)e^{-\epsilon^2 k_1 t}; \qquad k_1 \equiv 2 \frac{EB(AD+F)}{3(B+1)^{3/2}D},$$
(3.25)

where $x_1(0)$ is the initial position of the pulse and F is defined in (3.14). From (3.24a), we see that if $E = 0$, that is, if the pulse decays to a trivial background state, no pulse can exist unless $A > 0$. This is because the non-trivial background state of activator acts as a source for the inhibitor through the Bu term in (2.1b), and without this source, feed of the inhibitor must enter through boundaries. Further, for $E = 0$ and $A > 0$, (3.25) predicts that the pulse will remain stationary to all orders of ϵ. However, in this case, exponentially slow dynamics due to the failure of the pulse profile to satisfy the no-flux boundary conditions become important. This is analogous to the metastable pulse solution in a non-local reaction–diffusion equation derived from a certain limit of the Gierer–Meinhardt model (see [9]) and is addressed in Appendix A.

The evolution of two pulses centred at $(-\alpha(t), \alpha(t))$ can also be obtained explicitly, the evolution of $\alpha(t)$ given by

$$\alpha(t) = \left[\alpha(0) - \frac{AD+F}{2F} \right] e^{-\epsilon^2 k_2 t} + \frac{AD+F}{2F}; \qquad k_2 \equiv \frac{BE(AD+F)}{3(B+1)^{3/2}D}.$$
(3.26)

Comparing (3.26) to (3.25), we see that the evolution of a symmetric two-pulse pattern when $A = 0$ is simply that of a one pulse pattern on a domain of half the size. When $A > 0$, the equilibrium locations of the pulses are given by $\alpha = (AD+F)/(2F)$ so that when A exceeds the critical value A_{c_2} given by

$$A_{c_2} = \frac{F}{D},$$
(3.27)

equilibrium locations of the pulses are outside of the domain. We will illustrate the importance of this threshold below.

For a three-pulse pattern symmetric about $x = 0$ with pulses located at $(x_1(t), x_2, x_3(t)) = (-\alpha(t), 0, \alpha(t))$, we argue by symmetry that $\bar{V}_1 = \bar{V}_3 \equiv \bar{V}$. Then, the evolution of $\alpha(t)$ is given by

$$\frac{d\alpha}{dt} = \epsilon^2 \frac{2}{\bar{V}} \left(-\alpha \frac{F}{D} + A + \frac{F}{D} - \frac{3\sqrt{B+1}}{\bar{V}D} \right),$$
(3.28)

where $\bar{V}$ is solved in terms of α using (3.22). As we discuss in Section 5, only symmetric patterns are stable; thus, in equilibrium, all pulse amplitudes are equal so that $\bar{V}_i = 9\sqrt{B+1}/(AD+F)$, $i = 1, 2, 3$. Applying this in (3.28), we find that in equilibrium $\alpha = 2(AD+F)/(3F)$, leading to the three-pulse threshold for existence of equilibrium

locations inside the domain

$$A_{c_3} = \frac{F}{2D}. \tag{3.29}$$

When the boundary feed exceeds the respective thresholds above, pulses at the edges of the pattern are captured by the boundary. Thus, whereas when the boundary feed rate is sufficiently small, the boundaries repel the pulses, when the boundary feed is sufficiently large, the boundaries become attractive, leading to equilibrium patterns where pulses are centred at the boundary. We illustrate this point in the figures below in which we compare asymptotic results to those obtained numerically from solving (2.1) using the MATLAB function pdepe(). The locations of the centres of the pulses are simply taken to be the locations on the grid where local maxima of u occur; we do not perform an interpolation near the maxima to compute a more accurate location. The asymptotic results may be obtained from either numerically solving the DAE (3.22) and (3.23) with (3.19), or from (3.26) and (3.28). In all plots containing u and v, the plotted quantities are $\epsilon^{1/2}u$ (solid line) and $\epsilon^{-1/2}v$ (dashed line). Lastly, in plots comparing the asymptotic prediction of the pulse location(s), the solid line represents the numerical result while the circles represent the asymptotic result.

In Figures 1(a)–(c), we show the case of repulsive boundaries resulting from $A < A_{c_2}$. Figure 1(a) shows the quasi-equilibrium initial conditions for u and v. In Figure 1(b), we compare the asymptotic prediction of the pulse locations to that of the numerical solution. As predicted, the pulses evolve to symmetric equilibrium locations inside the domain as seen in Figure 1(c). Note that, as expected, locations of activator maxima coincide with locations of inhibitor minima. Figures 1(d)–(f) show the $A > A_{c_2}$ case for attractive boundaries. In Figure 1(d), we see that the asymptotic prediction of the pulse locations is accurate until the pulses become sufficiently close to the boundary, at which point the asymptotic results become invalid. Figure 1(e) shows the evolution of the right pulse as it approaches and is captured by the boundary at $x = 1$. From the times given in the caption, it is seen that the capture process is rapid relative to the evolution of the pulse when sufficiently far from the boundary. During this time as the pulse approaches the boundary, its amplitude doubles. Thus, as the pulses approach the boundaries, their amplitudes change dramatically in a short time. Lastly, we plot the equilibrium pattern in Figure 1(f) with two pulses centred at the boundary with twice their original amplitudes due to the fact that only half of each pulse is inside the domain. The Neumann conditions for v are met by boundary layers near $x = \pm 1$.

In Figures 2(a)–(c), we show the case of attracting boundaries for a three-pulse example symmetric about $x = 0$. The centre pulse remains stationary, while the two edge-pulses drift towards the boundaries. As before, the asymptotics are able to predict the evolution of the pulses until they are too close to the boundaries (Figures 2(a) and (b)). In contrast to the two-pulse case, the pulse amplitudes must be calculated as a function of the pulse locations, and thus, vary in time (Figure 2(b)). The difference between the asymptotic and numerical results in Figure 2(b) can be attributed to not including the second term in the expansion for u in (3.1). In Figure 2(c), we show the equilibrium state with one pulse in the centre and two pulses centred at the boundaries.

In further numerical computations (not shown), we observed that any quasi-equilibrium pattern evolves to a symmetric equilibrium as long as pulses are not captured by the
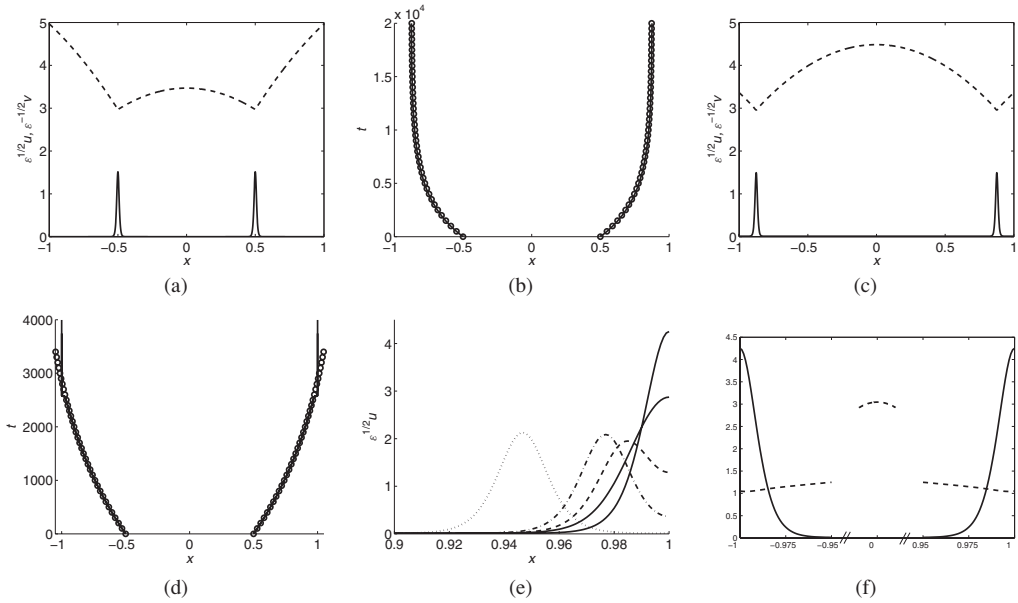
FIGURE 1. Illustration of the effect of boundary feed rate on the behaviour of boundaries with $\epsilon = 0.01$, $B = 2$, $D = 0.5$ and $E = 3$ so that $A_{c_2} = 4$. In (a)–(c), $A = 3$ while in (d)–(f), $A = 6$. In both cases, the initial conditions (plotted for the former case in (a)) are $(x_1, x_2) = (-0.5, 0.5)$. When $A < A_{c_2}$, the boundaries are repulsive and the pulses evolve to equilibrium locations inside the domain ((b) and (c)). When $A > A_{c_2}$, the boundaries are attractive so that the pulses are captured by the boundaries ((d) and (f)). Note that the axis breaks in (f). In (e), we show the evolution of the right pulse as it propagates to the right towards boundary at $x = 1$. The dotted line is a snapshot of $\epsilon^{1/2}u$ taken at $t = 2341$, the dashed-dotted line at $t = 2561$ and the dashed line at $t = 2576$. The two solid lines correspond to $t = 2577$ and $t = 2583$, the taller pulse being the equilibrium shape.
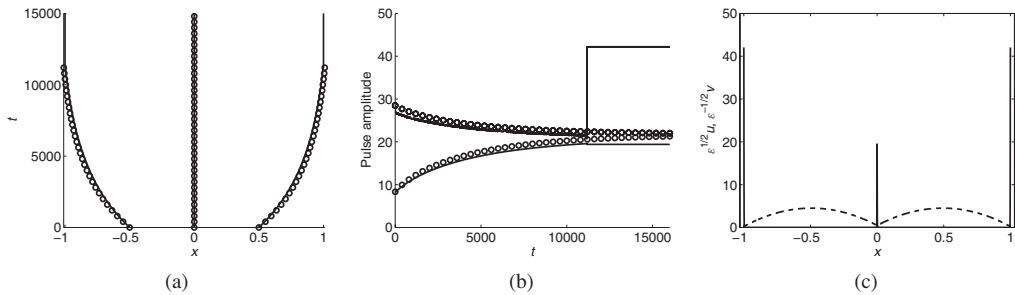

FIGURE 2. Illustration of the effect of boundary feed rate on the behaviour of boundaries with $\epsilon = 0.00125$, $B = 5$, $D = 1$ and $E = 40$ so that $A_{c_3} = 16.67$. Here, $A = 20 > A_{c_3}$ so that the two edge-pulses are captured by the boundary. In (a) and (b), we compare the asymptotic to numerical results for pulse locations and amplitudes. In (c), we plot the equilibrium state with two pulses centred on the boundary.

boundaries (rapid pulse collapse events, discussed briefly in Section 6, leading to a decrease in the number of pulses are possible, though are not studied in this paper). In the next section, we construct such equilibria by deriving an algebraic system from equilibrium points of the DAE obtained in this section. In addition, we construct asymmetric equilibria characterised by pulses of different amplitudes and find conditions for their existence.

4 Symmetric and asymmetric equilibria

In this section, we construct equilibrium states of (2.1) by finding equilibrium solutions of the DAE (3.22)–(3.23). By (3.23), equilibrium solutions for x_i, $\bar{V}_i$, $i = 1\dots, N$, and $\bar{v}$ must satisfy the system (3.22) along with $c_{i_1} = 0$, $i = 1,\dots, N$, where c_{i_1} is given in (3.19). We begin by considering symmetric equilibria for which all pulse amplitudes have a common value, but for which inter-pulse spacing may be non-uniform in the presence of a boundary feed rate. We will find that a positive boundary feed rate increases both the pulse amplitudes as well as inter-pulse spacing. Also, in particular, we derive a threshold for the boundary feed rate at which the interaction between the boundary and the edge pulses changes from repulsive to attractive. In previous similar studies with no boundary feed, the boundaries were shown to be repulsive. The other main focus of this section is to show that, in addition to symmetric equilibria, there exist asymmetric equilibria in which the pulse amplitudes can differ from one another. The existence of asymmetric equilibria arises from the multi-valued property of the inverse of a function obtained from solving (3.22) and $c_{i_1} = 0$. No general statement can be made about the effect of boundary feed on asymmetric equilibria; its effect depends on specific cases and will not be discussed here.

We begin by obtaining a general relation between equilibrium pulse locations and their amplitudes, applicable to both symmetric and asymmetric patterns. We then consider the two cases separately. Using (3.20) for c_{i_1}, we obtain

$$\frac{3b}{D\bar{V}_i} + Ax_i + 6b \sum_{j=1}^{N} \frac{1}{\bar{V}_j} G_x(x_i^-; x_j) = 0, \tag{4.1}$$

where

$$b \equiv \sqrt{B+1}. \tag{4.2}$$

Using

$$G_x(x; x_j) = -\frac{x}{2D} + \frac{1}{2D}\,\text{sgn}(x - x_j)$$

in (4.1), we find that the equilibrium pulse locations satisfy

$$\frac{1}{\bar{V}_i} - x_i \sum_{j=1}^{N} \frac{1}{\bar{V}_j} + \sum_{j=1}^{N} \frac{1}{\bar{V}_j}\,\text{sgn}(x_i^- - x_j) = -\frac{AD}{3b}x_i. \tag{4.3}$$

Using (3.22b) for the first sum in (4.3), and defining ℓ_j in terms of $\bar{V}_j$ by

$$\bar{V}_j = \frac{3b}{(AD+F)\ell_j}, \tag{4.4}$$

we split the second sum in (4.3) according to $\text{sgn}(x - x_j)$ and simplify to find

$$\ell_i + \sum_{j=1}^{i-1} \ell_j - \sum_{j=i}^{N} \ell_j = Cx_i, \tag{4.5}$$

where

$$C \equiv \frac{F}{AD + F} \leqslant 1. \tag{4.6}$$

Note that equality in (4.6) holds if $A = 0$. We make two remarks about ℓ_j. First, since $\bar{V}_j$ is inversely proportional to the amplitude of pulse j, ℓ_j is proportional to the amplitude. Second, the equivalent statement to (3.22b) in terms of ℓ_j is

$$\sum_{j=1}^{N} \ell_j = 1, \tag{4.7}$$

which we use to write the second sum in (4.5) in terms of the first sum to calculate an expression for x_i in terms of ℓ_j, $j \leqslant i$:

$$x_i = \frac{1}{C} \left(2 \sum_{j=1}^{i-1} \ell_j - 1 + \ell_i \right). \tag{4.8}$$

From (4.8), we obtain the recursion relation for the pulse locations

$$x_1 = \frac{1}{C}(-1 + \ell_1), \quad x_{i+1} = x_i + \frac{1}{C}(\ell_i + \ell_{i+1}), \quad x_N = \frac{1}{C}(1 - \ell_N). \tag{4.9}$$

If $C = 1$, the quantity $2\ell_j$ can be interpreted as the space occupied by pulse j. This interpretation was used in [30] to construct asymmetric pulse equilibria to the zero-boundary-flux Schnakenberg model, where equilibrium solutions allowed for pulses of two different amplitudes. The method of constructing the asymmetric equilibria was different from that employed in this section, as single pulses solved for on a domain of length $2\ell_j$ were 'glued' together to form a multi-pulse solution. That method does not extend as naturally here because we allow for non-homogeneous boundary conditions. However, we will see below that asymmetric equilibria of the Brusselator model arise in the same manner as in the Schnakenberg model.

We first consider the simple case of symmetric solutions. Since all pulse amplitudes are equal, (4.7) yields $\ell_j = 1/N$ for all $j = 1, \ldots, N$, leading to $\bar{V}_j = 3\sqrt{B+1}N/(AD+F)$. Since pulse amplitudes are inversely proportional to $\bar{V}_j$, we see that increasing boundary feed leads to increasing pulse amplitudes in the case of symmetric solutions. The recursion relation (4.9) also simplifies, yielding

$$x_j = \frac{1}{C}\left(-1 + \frac{2j-1}{N}\right). \tag{4.10}$$

With C given in (4.6), it is evident from (4.10) that the presence of boundary feed increases inter-pulse spacing and also leads to equilibrium edge-pulse locations closer

to the boundaries. The condition for all pulses to be inside the domain is $x_N < 1$, or $C > (N-1)/N$. That is, as the boundary feed increases to some critical value A_{c_N}, the edge pulses become centred on the boundary, and as the feed is increased past this threshold, no equilibrium positions within boundaries exist for the edge pulses. In terms of the slow evolution of Section 3, the boundaries when $A > A_{c_N}$ are said to be attracting. This leads to the main result of this section.

Principal Result II *Let $\epsilon \to 0$ in (2.1) and assume $O(1)$ separation between adjacent pulses as well as $O(1)$ separation between edge pulses and nearest boundaries, and consider the slow evolution of the quasi-equilibrium pattern given in Principal Result I. Then, the threshold A_{c_N} for the boundary feed A at which the boundaries change from repelling to attracting the pulses at the edges of an N-pulse pattern $(N > 1)$ is given by*

$$A_{c_N} = \frac{F}{(N-1)D}. \tag{4.11}$$

When $A < A_{c_N}$, the boundaries repel pulses at the edges of the pattern, while when $A \geqslant A_{c_N}$, the boundaries attract the edge pulses.

We note that the result (4.11) is consistent with those obtained in (3.27) and (3.29) for the two- and three-pulse cases and also that $E > 0$ is required for equilibrium locations inside the boundaries to exist. Because it appears that all asymmetric equilibria are unstable, as we will discuss in Section 5, this analysis is not worth repeating for asymmetric solutions, as quasi-equilibrium patterns will always evolve towards symmetric equilibrium points.

To construct asymmetric equilibria, we compute ℓ_j using (3.22a) to find $N-1$ equations of the form

$$\bar{V}_{i+1} - 6b \sum_{j=1}^{N} \frac{1}{\bar{V}_j} G(x_{i+1}; x_j) - \frac{A}{2} x_{i+1}^2 = \bar{V}_i - 6b \sum_{j=1}^{N} \frac{1}{\bar{V}_j} G(x_i; x_j) - \frac{A}{2} x_i^2, \quad i = 1, \ldots, N-1. \tag{4.12}$$

Using (4.4) to write $\bar{V}_j$ in terms of ℓ_j, (4.12) becomes

$$\frac{3b}{AD+F} \left(\frac{1}{\ell_{i+1}} - \frac{1}{\ell_i} \right) = 2(AD+F) \sum_{j=1}^{N} \ell_j (G(x_{i+1}; x_j) - G(x_i; x_j)) + \frac{A}{2} \left(x_{i+1}^2 - x_i^2 \right). \tag{4.13}$$

We calculate the sum in (4.13) to be

$$\sum_{j=1}^{N} \ell_j (G(x_{i+1}; x_j) - G(x_i; x_j)) = -\frac{1}{4D} \left(x_{i+1}^2 - x_i^2 \right) + \frac{1}{2CD} (\ell_i + \ell_{i+1}) \left(\sum_{j=1}^{i} \ell_j - \sum_{j=i+1}^{N} \ell_j \right). \tag{4.14}$$

To write the difference of squares term in (4.14) in terms of ℓ_i and ℓ_{i+1}, we write

$$x_{i+1}^2 - x_i^2 = (x_{i+1} - x_i)(x_{i+1} - x_i + 2x_i) = (x_{i+1} - x_i)^2 + 2x_i(x_{i+1} - x_i),$$
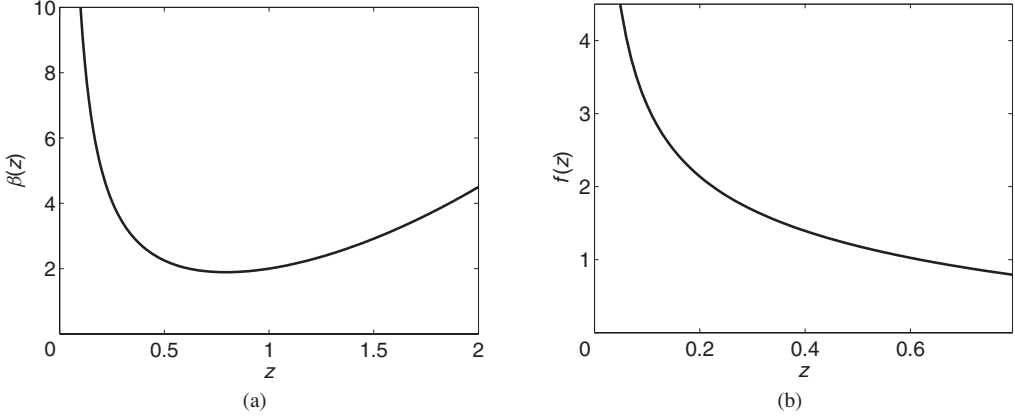
FIGURE 3. Plots of the functions $\beta(z)$ (a) and $f(z)$ (b). The domain over which $f(z)$ is plotted is $z \in (0, z_c)$.

and, upon applying (4.8) for x_i and (4.9) for $(x_{i+1} - x_i)$, we find that

$$x_{i+1}^2 - x_i^2 = \frac{1}{C^2}(\ell_{i+1} + \ell_i)\left(4\sum_{j=1}^{i}\ell_j + \ell_{i+1} - \ell_i - 2\right). \tag{4.15}$$

Using (4.15) and (4.14) in (4.13) and recalling (4.7), we find that, upon rearranging,

$$\frac{1}{\ell_{i+1}} - \frac{1}{\ell_i} = \frac{(AD + F)^3}{6bDF}(\ell_i^2 - \ell_{i+1}^2). \tag{4.16}$$

Making the substitution

$$\ell_i = qz_i, \qquad q \equiv \frac{(6bDF)^{1/3}}{AD + F}, \tag{4.17}$$

in (4.16) and (4.7), we find that z_i must satisfy

$$\beta(z_i) = \beta(z_{i+1}), \qquad i = 1, \dots, N - 1, \tag{4.18a}$$

$$\sum_{j=1}^{N} z_j = \frac{1}{q}, \tag{4.18b}$$

where $\beta(z) \equiv z^2 + \frac{1}{z}$. Note that the amplitude of pulse j is proportional to z_j. The function $\beta(z)$, plotted for a select range of z in Figure 3(a), has a global minimum at $z = z_c$, where

$$z_c = 2^{-1/3}. \tag{4.19}$$

Further, $\beta'(z) < 0$ on $(0, z_c)$ and $\beta'(z) > 0$ on (z_c, ∞). Thus, for any $z \in (0, z_c)$, there exists a unique point $\tilde{z} \in (z_c, \infty)$ such that $\beta(z) = \beta(\tilde{z})$. That is, the inverse function $\beta^{-1}(z)$ is multi-valued. Consequently, because (4.18a) must be satisfied for $i = 1, \dots, N - 1$, z_i can take on two and only two possible values, yielding two possible pulse amplitudes in a given equilibrium state. It is not restricted, however, in which value it does take on,

meaning that the left-to-right order in which the pulses appear in the domain is arbitrary. Since the amplitude of pulse i is proportional to z_i, $z_i = z$ would correspond to a small pulse at location i, while $z_i = \tilde{z}$ would correspond to a large pulse at location i. The system (4.18) is the same system that also led to the possibility of two-pulse amplitudes in equilibrium solutions constructed in [30].

To find solutions to (4.18), we first solve $\beta(\tilde{z}) = \beta(z)$ for $\tilde{z} > z$ in terms of z. There are two positive solutions for $\tilde{z}$; clearly one solution is $\tilde{z} = z$. The other is given by

$$\tilde{z} = f(z) = \frac{-z + \sqrt{z^2 + 4/z}}{2} > z.$$

The function $f(z)$ is plotted in Figure 3(b).

Letting N_1 be the number of small pulses and $N_2 = N - N_1$ be the number of large pulses, allowing (4.18b) to be written as $N_1 z + N_2 \tilde{z} = 1/q$, we find that an equilibrium solution exists if there is at least one intersection between the curves

$$\tilde{z} = -\frac{N_1}{N_2} z + \frac{1}{qN_2}, \tag{4.20a}$$

$$\tilde{z} = \frac{-z + \sqrt{z^2 + 4/z}}{2}. \tag{4.20b}$$

Analysis concerning the existence and uniqueness of solutions to (4.20) can be found in [30]. We give here a short discussion leading to the results. The important properties of the function $f(z)$ are that $f(z_c) = z_c$, $f''(z) > 0$ on $(0, z_c)$, $f'(0) = -\infty$ and $f'(z_c) = -1$. We can then conclude that $f'(z) < -1$ on $(0, z_c)$. Thus, if $N_1/N_2 \leqslant 1$, there can be at most one intersection between the two curves in (4.20) in the interval $z \in (0, z_c)$. For a given N_1 and N_2, the value of $\tilde{z}$ at which the intersection occurs decreases as q increases; that is, the line (4.20a) shifts downwards as q increases. As q increases above a critical value q_m, the two curves can no longer intersect. When $q = q_m$, the intersection occurs at $(z, \tilde{z}) = (z_c, z_c)$. Using this fact in (4.20a), we find that

$$q_m = \frac{1}{Nz_c}, \tag{4.21}$$

where $N = N_1 + N_2$ is the total number of pulses, and z_c is given in (4.19). The intersection of the two curves at $(z, \tilde{z}) = (z_c, z_c)$ when $q = q_m$ leads to the small and large pulses being of equal amplitude. Thus, when $N_1 \leqslant N_2$, asymmetric equilibria exist only when $q < q_m$.

If $N_1/N_2 > 1$, there can be either zero, one or two points of intersection in the interval $z \in (0, z_c)$. The three ways in which intersections can occur are depicted for $N_1 = 3$ and $N_2 = 1$ in Figure 4. Similar to the previous case, as q increases past a critical value q_{m_1}, no intersection is possible. When $q = q_{m_1}$, the two curves are tangent at $z = z_*$ (the bottommost curve in Figure 4), where $0 < z_* < z_c$ is given by

$$z_* = \left[\frac{2(1 + \gamma^2) - 2\sqrt{(1 + \gamma^2)^2 - (1 - \gamma^2)}}{(1 - \gamma^2)} \right]^{1/3}, \quad \gamma = 1 - \frac{2N_1}{N_2}. \tag{4.22}$$
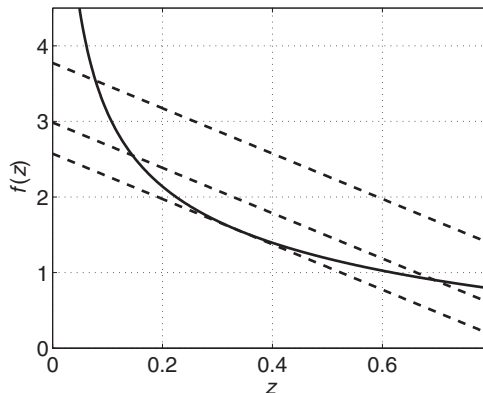
FIGURE 4. Plot of $f(z)$ (solid curve) and the linear function (4.20a) (dashed lines) for $N_1 = 3$, $N_2 = 1$. When $q = q_{m_1}$, the two curves are tangent. When $q_m < q < q_{m_1}$, there are two intersections and when $q < q_m$, there is only one intersection. Here, $q_m \approx 0.31498$ and $q_{m_1} \approx 0.3886$. The three values of q, from lowest line to highest line, are $q \approx 0.3886$, $q \approx 0.33498$ and $q \approx 0.26498$.

Using (4.22) in (4.20a), we obtain the expression for q_{m_1}

$$q_{m_1} = \frac{1}{N_1 z_* + N_2 f(z_*)}. \tag{4.23}$$

As q decreases below q_{m_1}, the curves intersect in two locations (the middle line in Figure 4) until the rightmost intersection point reaches $(z, \tilde{z}) = (z_c, z_c)$. The value of q at which this occurs is $q = q_m$. For $q < q_m$, only one intersection on $z \in (0, z_c)$ is possible (the uppermost line in Figure 4).

We now summarise the results of asymmetric equilibria. The forms of u and v are the same as those of the quasi-equilibrium solution given in (3.21), where the pulse locations x_j are given by the recursion relation (4.9), with $\ell_j = qz$ corresponding to a small pulse centred at $x = x_j$, or $\ell_j = q\tilde{z}$ corresponding to a large pulse centred at $x = x_j$. Here, q is defined in (4.17), and $(z, \tilde{z})$ is given by an intersection of the right-hand sides of (4.20a) and (4.20b). The inverse proportionality constant of the amplitude of each pulse, $\bar{V}_j$, is given in terms of ℓ_j by (4.4). The last parameter needed to construct the solution is $\bar{v}$, which may be calculated from x_j and $\bar{V}_j$ independent of i from (3.22a). The left-to-right ordering of small and large pulses is arbitrary.

In Figures 5(a) and (b), we demonstrate the arbitrary left-to-right ordering of small and large pulses using a five-pulse example with $N_1 = 2$ and $N_2 = 3$. Even though the same parameters were used to generate Figures 5(a) and (b), the arbitrary left-to-right ordering predicted above allows for different equilibrium states. However, since $N_1 < N_2$, only two possible pulse amplitudes are possible. That is, while other left-to-right orderings are possible, the pulse amplitudes in Figure 5 are the only amplitudes allowed by the parameter set.

In Figures 6(a) and (b), we demonstrate the non-uniqueness of the solutions to (4.20) when $N_1 > N_2$. We illustrate the point on a four-pulse example with $N_1 = 3$ and $N_2 = 1$. The parameters are the same as those used to generate the middle line in Figure 4. With the same left-to-right ordering of small and large pulses, we plot the solutions
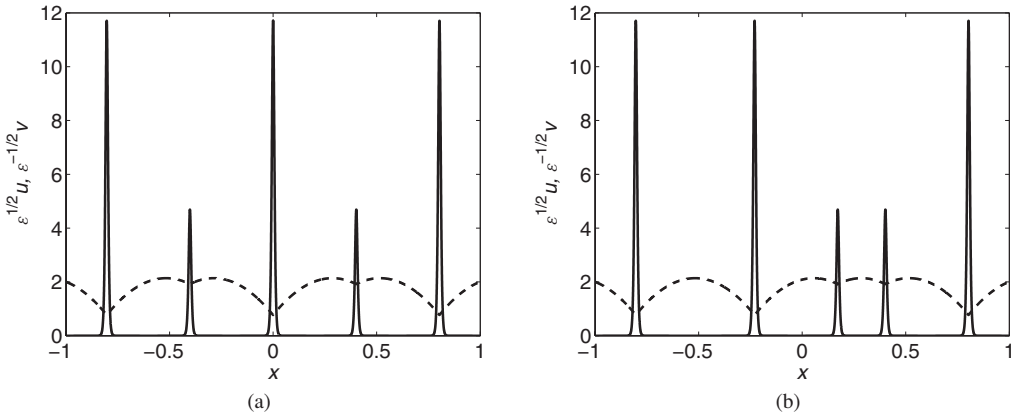
FIGURE 5. Two asymmetric equilibrium states with $N_1 = 2$ and $N_2 = 3$ and the same parameters but different left-to-right ordering of small and large pulses. The parameters are $\epsilon = 0.01$, $A = 3$, $B = 5$, $D = 1$ and $E = 40$. The small and large pulses of (a) are of the same amplitude as those in (b).
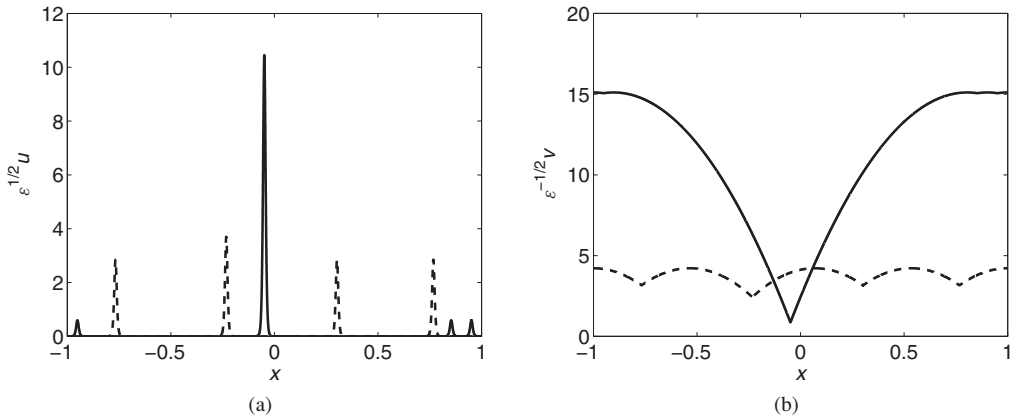

FIGURE 6. Four-pulse asymmetric solutions with $N_1 = 3$ and $N_2 = 1$ and the same left-to-right ordering but corresponding to different intersections of $f(z)$ and the middle curve of Figure 4. The parameters are $\epsilon = 0.01$, $A = 0$, $B = 5$, $D \approx 0.25576$ and $E = 12$ so that $q_m \approx 0.31498$, $q_{m_1} \approx 0.3886$ and $q \approx 0.34498$. We plot $\epsilon^{1/2}u$ in (a) and $\epsilon^{-1/2}v$ in (b). The solid curves correspond to the left intersection, while the dashed curves correspond to the right intersection.

corresponding to the left (solid) and right (dashed) intersections in Figure 4. The left intersection corresponds to more disparate values for z and $\tilde{z}$, leading to more disparate pulse amplitudes and inter-pulse spacings while the right intersection corresponds to less disparate values for z and $\tilde{z}$, and thus, the pulse amplitudes are less disparate with the pulses more evenly distributed across the domain.

In Section 5, we analyse the stability of N-pulse equilibria to small ($O(\epsilon^2)$) eigenvalues corresponding to perturbations that either grow or decay on an $O(\epsilon^2)$ time scale. They do not account for pulse collapse events in which one or more pulses collapse relatively

rapidly on an $O(1)$ time scale, nor do they predict oscillations of pulse amplitudes. Such instabilities are governed by large ($O(1)$) eigenvalues and are not studied here.

5 Stability of equilibria to small eigenvalues

In this section, we study the stability of the equilibrium solutions constructed in Section 4 to $O(\epsilon^2)$ eigenvalues. The class of perturbations that we consider accounts only for slow drift instabilities that occur on an $O(\epsilon^2)$ time scale; analysis of these perturbations cannot predict instabilities that occur on an $O(1)$ time scale. Thus, stability with respect to this class of perturbations does not guarantee that such solutions are stable though solutions found to be unstable to these perturbations are certainly unstable. Two approaches were taken to analyse the stability to such perturbations. The first approach in which an eigenvalue problem is derived by linearising the system (2.1) around an N-pulse equilibrium solution is analogous to that taken in the small eigenvalue analysis of [30]. As in [30], we found that the eigenvalues scaled as $O(\epsilon^2)$ and were eigenvalues of a certain $N \times N$ matrix $\mathcal{M}_P$. In the other approach, instead of linearising (2.1), we linearise the DAE system (3.22)–(3.23) around an N-pulse equilibrium solution. The associated eigenvalues are eigenvalues of an $N \times N$ matrix $\mathcal{M}_D$. Since the DAE evolves on an $O(\epsilon^2)$ time scale, perturbations of the DAE also grow or decay on an $O(\epsilon^2)$ time scale, consistent with the first approach. Moreover, further calculations (not shown) show that $\mathcal{M}_D = r\mathcal{M}_P$, where r is a positive constant. The two analyses thus yield the same results in terms of stability and are equivalent. Because of the length of the first analysis and its similarity to that given in [30], we only present the stability analysis of the DAE in this section.

We first introduce the N-dimensional column vectors $\mathbf{x} = (x_1, \ldots, x_N)^{\mathrm{T}}$ and $\mathbf{V} = (\bar{V}_1, \ldots, \bar{V}_N)^{\mathrm{T}}$ containing the pulse locations and inverse pulse amplitudes, respectively, where T denotes the transpose. We also denote

$$\mathbf{C}(\mathbf{x}, \mathbf{V}) = (C_1(\mathbf{x}, \mathbf{V}), \ldots, C_N(\mathbf{x}, \mathbf{V}))^{\mathrm{T}}, \tag{5.1a}$$

$$C_i(\mathbf{x}, \mathbf{V}) \equiv c_{i_1} = -\frac{3b}{D\bar{V}_i} + Ax_i + 6b \sum_{j=1}^{N} \frac{1}{\bar{V}_j} G_x(x_i^+; x_j), \quad i = 1, \ldots, N, \tag{5.1b}$$

where c_{i_1} was defined in (3.19). We lastly rewrite the $N+1$ algebraic equations in (3.22) in vector form as

$$\mathbf{H}(\mathbf{x}, \mathbf{V}, \bar{v}) = 0, \quad S(\mathbf{V}) = 0,$$

where

$$\mathbf{H}(\mathbf{x}, \mathbf{V}, \bar{v}) = (H_1(\mathbf{x}, \mathbf{V}, \bar{v}), \ldots, H_N(\mathbf{x}, \mathbf{V}, \bar{v}))^{\mathrm{T}}, \tag{5.2a}$$

$$H_i(\mathbf{x}, \mathbf{V}, \bar{v}) = \bar{v} - \bar{V}_i + 6b \sum_{j=1}^{N} \frac{1}{\bar{V}_j} G(x_i; x_j) + \frac{A}{2} x_i^2, \quad i = 1, \ldots, N, \tag{5.2b}$$

and

$$S(\mathbf{V}) = \sum_{j=1}^{N} \frac{1}{\bar{V}_j} - \frac{AD + F}{3b},$$

with F defined in (3.14) and b defined in (4.2). An equilibrium solution $(\mathbf{x}, \mathbf{V}, \bar{v}) = (\mathbf{x}_e, \mathbf{V}_e, \bar{v}_e)$ thus satisfies the $2N + 1$ system of equations

$$\mathbf{C}(\mathbf{x}_e, \mathbf{V}_e) = 0, \qquad (5.3a)$$

$$\mathbf{H}(\mathbf{x}_e, \mathbf{V}_e, \bar{v}_e) = 0, \qquad (5.3b)$$

$$S(\mathbf{V}_e) = 0. \qquad (5.3c)$$

To derive the eigenvalue problem that determines stability, we perturb the equilibrium solutions according to

$$\mathbf{x} = \mathbf{x}_e + \delta\boldsymbol{\xi}, \quad \mathbf{V} = \mathbf{V}_e + \delta\boldsymbol{\phi}, \quad \bar{v} = \bar{v}_e + \delta\mu, \qquad (5.4)$$

with $\delta \ll 1$. We then use (5.3b) and (5.3c) to determine $\boldsymbol{\phi}$ and μ in terms of $\boldsymbol{\xi}$, which we then use in (5.3a) to compute $\mathbf{C}(\mathbf{x}, \mathbf{V}) = \delta\mathcal{M}\boldsymbol{\xi}$ for some matrix $\mathcal{M}$. Using this for $\mathbf{C}$ in (3.23), the leading order terms yield the eigenvalue problem $d\boldsymbol{\xi}/dt = 2\epsilon^2 \mathscr{V}^{(e)}\mathcal{M}\boldsymbol{\xi}$, where $\mathscr{V}^{(e)}$ is the matrix

$$\mathscr{V}^{(e)} \equiv \begin{pmatrix} 1/\bar{V}_{1e} & 0 & \dots & 0 \\ 0 & \ddots & \dots & 0 \\ \vdots & \vdots & \ddots & \vdots \\ 0 & 0 & \cdots & 1/\bar{V}_{Ne} \end{pmatrix}, \qquad (5.5)$$

where V_{ie} is the ith component of $\mathbf{V}_e$. The eigenvalues of the matrix $\mathscr{V}^{(e)}\mathcal{M}$ then determine the stability of the equilibrium solutions with respect to perturbations of the DAE.

We begin by substituting the perturbed solutions (5.4) into (5.3b) and expanding to first order in δ to calculate that

$$\mathscr{H}_{\mathbf{x}}^{(e)}\boldsymbol{\xi} + \mathscr{H}_{\mathbf{V}}^{(e)}\boldsymbol{\phi} + \mu\mathbf{H}_{\bar{v}}^{(e)} = 0, \qquad (5.6)$$

where, for some N-dimensional column vector $\mathbf{w}$, scalar s and N-dimensional vector function $\mathbf{F}$, $\mathscr{F}_{\mathbf{w}}(\mathbf{w}, s)$ denotes the Jacobian matrix

$$(\mathscr{F}_{\mathbf{w}}(\mathbf{w}, s))_{ij} = \frac{\partial F_i}{\partial w_j}, \quad 1 \leqslant i, j \leqslant N; \quad \mathbf{F} = (F_1, \dots, F_N)^{\mathrm{T}}, \quad \mathbf{w} = (w_1, \dots, w_N)^{\mathrm{T}},$$

and $\mathbf{F}_s$ denotes the derivative of $\mathbf{F}$ with respect to s, $(\mathbf{F}_s)_i = \frac{\partial F_i}{\partial s}$. The superscript $^{(e)}$ indicates that the quantity is evaluated at the equilibrium solution $(\mathbf{x}, \mathbf{V}, \bar{v}) = (\mathbf{x}_e, \mathbf{V}_e, \bar{v}_e)$. Next, expanding (5.3c) to first order in δ, we find that $\nabla S^{(e)\mathrm{T}}\boldsymbol{\phi} = 0$.

Since we require $\boldsymbol{\phi}$ in terms of $\boldsymbol{\xi}$, we must first calculate μ in terms of $\boldsymbol{\xi}$. We first use (5.6) to write

$$\boldsymbol{\phi} = -\mathscr{H}_{\mathbf{V}}^{(e)-1}\left(\mathscr{H}_{\mathbf{x}}^{(e)}\boldsymbol{\xi} + \mu\mathbf{e}_N\right), \qquad (5.7)$$

where we have used (5.2) to calculate that $\mathbf{H}_{\bar{v}}^{(e)}$ is the N-dimensional vector $\mathbf{e}_N \equiv (1, \dots, 1)^{\mathrm{T}}$. Then, using (5.7) for $\boldsymbol{\phi}$ in $\nabla S^{(e)\mathrm{T}}\boldsymbol{\phi} = 0$, we find that

$$\mu = -\frac{\nabla S^{(e)\mathrm{T}}\left(\mathscr{H}_{\mathbf{V}}^{(e)-1}\mathscr{H}_{\mathbf{x}}^{(e)}\boldsymbol{\xi}\right)}{\nabla S^{(e)\mathrm{T}}\mathscr{H}_{\mathbf{V}}^{(e)-1}\mathbf{e}_N}. \qquad (5.8)$$

Using (5.8) for μ in (5.6), we arrive at

$$\mathscr{H}_\mathbf{V}^{(e)}\boldsymbol{\phi} = -\mathscr{H}_\mathbf{x}^{(e)}\boldsymbol{\xi} + \frac{\nabla \mathbf{S}^{(e)\mathrm{T}}\left(\mathscr{H}_\mathbf{V}^{(e)-1}\mathscr{H}_\mathbf{x}^{(e)}\boldsymbol{\xi}\right)}{\nabla \mathbf{S}^{(e)\mathrm{T}}\mathscr{H}_\mathbf{V}^{(e)-1}\mathbf{e}_N}\mathbf{e}_N,$$

which, upon some matrix algebra, yields $\boldsymbol{\phi} = \mathscr{R}\boldsymbol{\xi}$, where $\mathscr{R}$ is defined as

$$\mathscr{R} = \mathscr{H}_\mathbf{V}^{(e)-1}\left[-\mathscr{H}_\mathbf{x}^{(e)} + \frac{1}{\nabla \mathbf{S}^{(e)\mathrm{T}}\mathscr{H}_\mathbf{V}^{(e)-1}\mathbf{e}_N}\mathbf{e}_N\left(\nabla \mathbf{S}^{(e)\mathrm{T}}\mathscr{H}_\mathbf{V}^{(e)-1}\mathscr{H}_\mathbf{x}^{(e)}\right)\right]. \tag{5.9}$$

Finally, to derive the eigenvalue problem, we rewrite (3.23) in matrix form as

$$\frac{d\mathbf{x}}{dt} = 2\epsilon^2 \mathscr{V}\mathbf{C}(\mathbf{x}, \mathbf{V}), \qquad \mathscr{V} \equiv \begin{pmatrix} 1/\bar{V}_1 & 0 & \dots & 0 \\ 0 & \ddots & \dots & 0 \\ \vdots & \vdots & \ddots & \vdots \\ 0 & 0 & \dots & 1/\bar{V}_N \end{pmatrix}, \tag{5.10}$$

where $\mathbf{C}$ is defined in (5.1). Using the perturbations (5.4) for $\mathbf{x}$ and $\mathbf{V}$ in (5.10) and expanding to the first order in δ, we arrive at the eigenvalue problem

$$\frac{d\boldsymbol{\xi}}{dt} = 2\epsilon^2 \mathscr{V}^{(e)}\mathscr{M}\boldsymbol{\xi}, \qquad \mathscr{M} \equiv \mathscr{C}_\mathbf{x}^{(e)} + \mathscr{C}_\mathbf{V}^{(e)}\mathscr{R}, \tag{5.11}$$

where $\mathscr{V}^{(e)}$ and $\mathscr{R}$ are defined in (5.5) and (5.9), respectively. This leads to the main result of this section.

Principal Result III *Let $\epsilon \to 0$ in (2.1) and assume $O(1)$ separation between adjacent pulses as well as $O(1)$ separation between edge pulses and nearest boundaries, and consider an equilibrium solution as constructed in Section 4 parameterised by $(\mathbf{x}, \mathbf{V}, \bar{v}) = (\mathbf{x}_e, \mathbf{V}_e, \bar{v}_e)$. Then, the solution is stable with respect to small eigenvalues if all eigenvalues of the matrix $\mathscr{V}^{(e)}\mathscr{M}$ have negative real parts. Here, $\mathscr{V}^{(e)}$ and $\mathscr{M}$ are defined in (5.5) and (5.11), respectively. It is unstable if at least one of the eigenvalues has positive real part. The entries of the vectors and matrices defined above are given as follows:*

$$\left(\mathscr{H}_\mathbf{x}^{(e)}\right)_{ij} = \begin{cases} \dfrac{6\sqrt{B+1}}{\bar{V}_{je}}\dfrac{\partial}{\partial x_j}G(x_{ie}; x_j)\Big|_{x_j=x_{je}}, & i \neq j, \\ Ax_{ie} + 6\sqrt{B+1}\displaystyle\sum_{k=1}^N\dfrac{1}{\bar{V}_{ke}}\dfrac{\partial}{\partial x_i}G(x_i; x_{ke})\Big|_{x_i=x_{ie}}, & i = j, \end{cases}$$

$$\left(\mathscr{H}_\mathbf{V}^{(e)}\right)_{ij} = -\delta_{ij} - \frac{6\sqrt{B+1}}{\bar{V}_{je}^2}G(x_{ie}; x_{je}),$$

where δ_{ij} is the Kronecker delta function, and

$$(\nabla \mathbf{S}^{(e)\mathrm{T}})_i = -\frac{1}{\bar{V}_{ie}^2}, \qquad \left(\mathscr{C}_\mathbf{V}^{(e)}\right)_{ij} = \delta_{ij}\frac{3\sqrt{B+1}}{D\bar{V}_{ie}^2} - \frac{6\sqrt{B+1}}{\bar{V}_{je}^2}G_x(x_{ie}^+; x_{je}), \qquad \left(\mathscr{C}_\mathbf{x}^{(e)}\right)_{ij} = -\delta_{ij}\frac{F}{D},$$

where F is defined in (3.14). This stability result is equivalent to that obtained from analysing perturbations within the original system (2.1).

While, as expected, the above analysis predicts that some symmetric solutions are stable, it predicts that some asymmetric solutions are also stable. However, when solving (2.1) numerically with such asymmetric solutions as initial conditions, we have observed in all cases a pulse collapse event in which one or more pulses collapse relatively rapidly on an $O(1)$ time scale. Thus, it appears that no asymmetric solutions are stable. In the symmetric case with $A = 0$, the matrix $\mathscr{V}^{(e)}\mathscr{M}$ reduces to a positive multiple of a matrix analysed in [12], the eigenvalues ω_j of which were calculated as

$$
\omega_1 = -\frac{N}{2D}, \qquad \omega_j = -\frac{N}{2D}\left[\frac{\left(1-\left(\frac{q_m}{q}\right)^3\right)\tan^2\left(\frac{\theta_j}{2}\right)}{\tan^2\left(\frac{\theta_j}{2}\right)-\left(\frac{q_m}{q}\right)^3\sec^2\left(\frac{\theta_j}{2}\right)}\right], \qquad j = 2,\ldots,N,
$$

where $\theta_j = \pi(j-1)/N$, $j = 2,\ldots,N$, and q and q_m are defined in (4.17) and (4.21), respectively. Thus, we find that w_2 crosses into the right-half plane on the real axis when q is increased from q_m^- to q_m^+. When $q = q_m$, there are $N-1$ eigenvalues equal to 0, equalling the number of asymmetric branches that bifurcate from the symmetric branch (ignoring the permutations in left-to-right ordering of small and large pulses). We note that, for q sufficiently larger than q_m, all eigenvalues w_j become negative. However, it has been observed that these symmetric solutions are unstable to relatively rapid pulse collapse events (Figure 8(c)). We note that increasing ϵ from $\epsilon = 0.01$ to $\epsilon = 0.015$ in Figure 8(c) did not change the time at which the middle pulse collapsed, indicating an $O(1)$ instability.

Note that the value $q = q_m$ at which stability changes is also the value at which asymmetric patterns bifurcate from a symmetric branch with $A = 0$. This is found to be true also for $A > 0$ and is illustrated in Figures 7(a) and (b), where we plot bifurcation diagrams for one and two pulses (see Figure 7(a)) and three pulses (see Figure 7(b)). The horizontal axis is the bifurcation parameter A, while the vertical axis is the norm defined by

$$
|u|_2 = \left[\sum_{i=1}^{N}\left(\frac{3(B+1)}{2\bar{V}_j}\right)^2\right]^{1/2}.
$$

In the annotations, s_N is the symmetric N-pulse branch, and a 101 label represents a *large–small–large* ordering of a three-pulse asymmetric pattern. Parts of the branch that are stable (unstable) to small eigenvalues are depicted by a solid (dashed) line. Note that permutations of such a pattern would trace out the same curve though we have plotted the curve for the permutations for which the pulse locations are between -1 and 1 for the values of A depicted. Lastly, A_m and A_{m_1} are values of A such that $q = q_m$ and $q = q_{m_1}$, respectively, where q, q_m and q_{m_1} are given in (4.17), (4.21) and (4.23), respectively. As previously stated in terms of q, stability of the symmetric branches changes at when $A = A_m$. In Figure 7(b), two 001 solutions exist in the interval $A_{m_1} < A < A_m$ as found in Section 4 for the $N_1 > N_2$ case. The lower branch corresponds to the solution of (4.20) with large z and small $\bar{z}$, while the opposite is true for the upper branch. The upper branch ends when the location of an edge-pulse is outside of the domain. If the 010
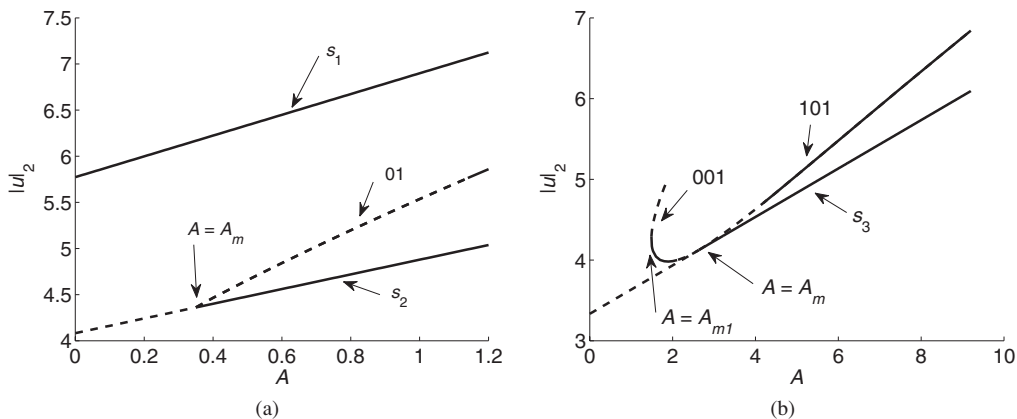
FIGURE 7. Bifurcation diagrams for one and two pulses (a) and three pulses (b) with $B = 2$ and $E = 10$. In (a), $D = 1.3$ while in (b), $D = 0.6$. The solid (dashed) lines indicate solutions that are stable (unstable) to slow instabilities. In (a), a single asymmetric branch (ignoring the 10 permutation) bifurcates from s_2 when $A = A_m$. In (b), two branches (again ignoring permutations) bifurcate from s_3 when $A = A_m$. In the region $A_{m_1} < A < A_m$, two 001 solutions exist.

solution were plotted instead, the stability properties of the branches would change. In all cases, asymmetric equilibria are unstable to small eigenvalues for A sufficiently near A_m, the value where they bifurcate from the symmetric branch. We emphasise that while some parts of asymmetric branches may be stable to small eigenvalues sufficiently far from the bifurcation point, numerical computations on (2.1) show that such solutions are unstable to rapid collapse events; we have not numerically observed a stable asymmetric solution. Lastly, in the context of the DAE, there is no contradiction in the existence of multiple stable equilibria for a given value of A; different solutions of the algebraic part of the DAE lead to different systems of differential equations whose stationary points (and their stability) are independent of one another.

In Figures 8(a) and (b), we show space–time plots of symmetric solutions starting from perturbations of two different three-pulse equilibria, both of which are stable to large eigenvalues, one for which $q < q_m$ (stable, Figure 8(a)) and the other for which $q > q_m$ (unstable, Figure 8(b)). The perturbation in the pulse locations was taken to be in the $(-1/\sqrt{2}, 0, 1/\sqrt{2})$ direction, with the perturbation in Figure 8(a) taken to be larger for illustrative purposes. In Figure 8(b), the solution drifts on an $O(\epsilon^2)$ time scale to a solution near a three-pulse asymmetric equilibrium observed numerically to be stable to large eigenvalues. However, because it is unstable to small eigenvalues, the pattern drifts for a duration of $O(\epsilon^{-2})$ until the pulse locations are such that the right pulse collapses (if the perturbation was in the $-(-1/\sqrt{2}, 0, 1/\sqrt{2})$ direction, it is the middle pulse that collapses). As was the case for the Gierer–Meinhardt model in [11], stability to collapse events is sensitive to instantaneous pulse locations; thus, in Figure 8(b), it is likely that the slow drift instability has triggered a fast collapse instability. While, as previously stated, the collapse event in Figure 8(c) occurs at a time independent of ϵ, the time of the collapse event in Figure 8(b) scales as $O(\epsilon^{-2})$, confirming that the initial instabilities in these two figures are of different nature. We finally note that all three-pulses drift in
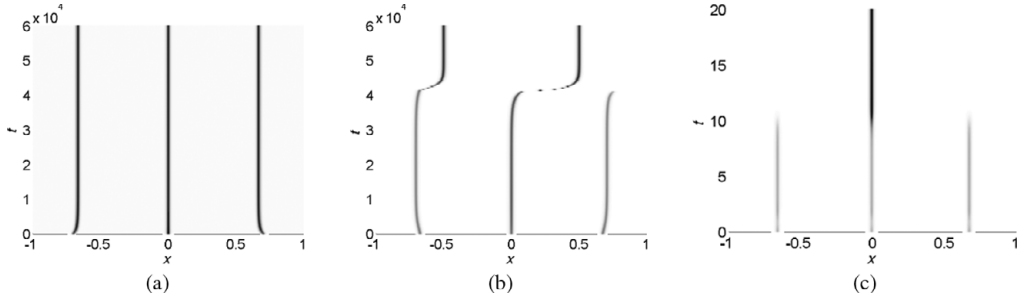
FIGURE 8. Space–time plot of $u(x,t)$ starting from perturbations of three-pulse equilibria. The dark (light) regions represent large (small) values. The parameters are $\epsilon = 0.01$, $A = 0$, $B = 2$ and $E = 10$. Here, $q_m \approx 0.41997$. The pulses are initially perturbed from their equilibrium locations at $(x_{1e}, x_{2e}, x_{3e}) = (-2/3, 0, 2/3)$. In (a), $D = 0.29$ ($q \approx 0.40778 < q_m$) so that the symmetric three-pulse equilibrium is stable. In (b), $D = 0.37$ ($q \approx 0.44228 > q_m$) so that the symmetric three-pulse equilibrium is unstable and the pulse locations drift away from the equilibrium locations. Eventually, one of the pulses collapses and the solution evolves to a stable two-pulse equilibrium ($q_m \approx 0.63 > q$). The apparent discontinuity near $t = 4 \times 10^4$ is due to the low temporal resolution used only for plotting purposes. In (c), $D = 2$ ($q \approx 0.7762$) so that $\omega_j < 0$ for $j = 1, 2, 3$. However, two pulses collapse relatively rapidly.

the same direction at the onset of the pulse collapse due to the fact that the unstable eigenvector ξ in (5.11) of the aforementioned asymmetric three-pulse equilibrium is in the $(0.38671, 0.83720, 0.38671)$ direction.

6 Conclusion

The method of matched asymptotic expansions was used to construct quasi-equilibrium pulse solutions to a singularly perturbed Brusselator model in the semi-strong pulse-interaction regime. We introduced a particular scaling of the parameters of the Brusselator model to analyse the regime in which pulses move towards equilibrium positions on an $O(\epsilon^2)$ time scale. Using solvability conditions and matching the inner and outer solutions, we derived a DAE for the evolution of the pulse locations and inverse pulse amplitudes. We found excellent agreement between the asymptotic and numerical results computed from the Brusselator equations. We observed that the presence of a boundary feed term shifted the equilibrium positions of the edge pulses towards the boundaries and increased inter-pulse spacings as well as pulse amplitudes. Further, based on the condition that edge pulses of an N-pulse symmetric equilibrium lie outside of the domain, we derived a critical boundary feed rate above which the pulse–boundary interaction changes from repulsive to attractive. When the boundary feed rate exceeded this threshold, we found that edge pulses of quasi-equilibrium solutions are captured by the boundary, leading to an equilibrium solution in which two pulses are centred at the boundary.

We also found equilibrium points of the DAE to construct equilibrium solutions. We found that, in addition to symmetric equilibria with equal pulse amplitudes, asymmetric solutions are also admitted for certain ranges of the parameter q defined in (4.17). The asymmetric equilibria are characterised by N_1 small and N_2 large pulses spaced unevenly

across the domain with arbitrary left-to-right ordering. Numerical evidence suggests that asymmetric equilibria are always unstable, resulting either in a slow evolution to a symmetric equilibrium or in the rapid collapse of one or more pulses.

Finally, we analysed the stability of N-pulse equilibria to perturbations that evolve on an $O(\epsilon^2)$ time scale. Calculations (not shown) reveal that analysing perturbations within the differential-algebraic system (3.22)–(3.23) is equivalent to analysing perturbations within the original reaction–diffusion system (2.1). Combining the stability results of Section 5 with those of numerical computations, we found that only symmetric solutions may be stable to both small and large eigenvalues and that asymmetric solutions appear to be always unstable to at least one of the modes of instability. Instability to large eigenvalues may manifest in rapid collapse events (depicted in Figure 8(c) for which the value of D is larger) or in pulse amplitude oscillations (not yet observed for this model). Study of such instabilities typically requires analysis of a non-local eigenvalue problem and has been performed for the Gierer–Meinhardt (see [10, 11, 31]) and Gray–Scott (see [16]) models. The study of large eigenvalues for the Brusselator model is an open problem. Another interesting problem might be to find if there exists a regime such that pulse-splitting behaviour may occur (as in, e.g. [17] and discussed qualitatively in [4]). It would also be interesting to study the evolution of spots in a two-dimensional singularly perturbed Brusselator model. In [19], spot replication was studied for a singularly perturbed Schnakenberg model on a unit square and unit disk.

Acknowledgements

Appendix A Exponentially slow evolution of a single pulse when $E = 0$ and $A > 0$

In Section 3, the analysis predicted that for the single-pulse case with $E = 0$ and $A > 0$, the pulse would remain stationary for all time regardless of its position in the domain. However, as we will show below, the single-pulse solution is in fact only metastable; the eigenvalue problem linearised around this solution admits an eigenvalue that is exponentially small but positive. We further find that the exponentially small eigenvalue is the principle eigenvalue, that is, the eigenvalue with the largest real part. Following closely the analysis of [9] for a particular limit of the Gierer–Meinhardt model, we begin by first casting (2.1) in the form of a non-local reaction–diffusion system and linearising around the quasi-equilibrium solution. We then analyse the resulting non-local eigenvalue problem and derive an asymptotic expression for the exponentially small (positive) eigenvalue. Numerical methods will be used to confirm the analysis as well as to show that no other eigenvalues have positive real parts. Finally, we derive an ODE for the exponentially slow dynamics of the centre of the pulse, which we confirm by numerically solving (2.1). Because the following analysis and arguments are similar to those in [9], we omit much of the detail.

For the purpose of the following analysis, it is convenient to consider a re-scaled form of (2.1). We introduce the new variables and parameters[1]

$$u = \epsilon^{-1/2}\frac{B}{A}U, \quad v = \epsilon^{1/2}AV, \quad t = \frac{1}{B+1}\tau, \quad \epsilon = \sqrt{B+1}\epsilon_0,$$

resulting in

$$U_\tau = \epsilon_0^2 U_{xx} + \epsilon_0 E_0 - U + fVU^2, \quad U_x(\pm 1, \tau) = 0, \tag{A 1a}$$

$$\sigma V_\tau = \mathscr{D}V_{xx} + \frac{1}{\epsilon_0}(U - VU^2) \quad V_x(\pm 1, \tau) = \pm 1, \tag{A 1b}$$

where

$$f = \frac{B}{B+1}, \quad E_0 = \frac{EA}{B\sqrt{B+1}}, \quad \mathscr{D} = D\sqrt{B+1}\frac{A^2}{B^2}, \quad (B+1)^{3/2}\frac{A^2}{B^2}.$$

We will consider the case where $E_0 = 0$ in (A 1a).

We assume as before that U has a localised solution of width $O(\epsilon_0)$ while V to leading order is equal to the constant $\bar{V}$ in the inner region and varies on an $O(1)$ length scale in the outer region. Then, in the outer region, treating functions of U as multiples of delta functions, (A 1b) must satisfy the Fredholm condition

$$\bar{V} = \frac{2\mathscr{D}\epsilon_0 + \int_{-1}^{1}U(x)\,dx}{\int_{-1}^{1}U^2(x)\,dx}.$$

Then, solving for the leading order solution of V in the outer region and matching it to the constant leading order inner solution, we write (A 1) as a non-local reaction–diffusion system

$$U_\tau = \epsilon_0^2 U_{xx} - U + fVU^2, \quad U_x(\pm 1, \tau) = 0, \tag{A 2a}$$

$$V = |x - x_0| + \frac{2\mathscr{D}\epsilon_0 + \int_{-1}^{1}U(x)\,dx}{\int_{-1}^{1}U^2(x)\,dx}, \tag{A 2b}$$

where we have set $E_0 = 0$. The leading order quasi-equilibrium solution is then

$$U_E(x; x_0) = \frac{1}{fV_0}u_c\left(\frac{x - x_0}{\epsilon}\right); \quad u_c(y) \equiv \frac{3}{2}\text{sech}^2\left(\frac{y}{2}\right),$$

$$V_E(x; x_0) = |x - x_0| + V_0; \quad V_0 \equiv \frac{3(1 - f)}{\mathscr{D}f^2},$$

where x_0 is the centre of the pulse.

To derive the eigenvalue problem, we linearise (A 2) around U_E and V_E by introducing perturbations ϕ and η according to

$$U = U_E(x; x_0) + e^{\lambda t}\phi(x), \tag{A 3a}$$

$$V = V_E(x; x_0) + e^{\lambda t}\eta, \tag{A 3b}$$

[1] This scaling was suggested to us by a reviewer.

where η is a constant. Substituting (A 3) into (A 2a), we obtain the following non-local eigenvalue problem:

$$L_{\epsilon_0}\phi \equiv \epsilon_0^2 \phi_{xx} + (-1 + 2u_c)\phi + \frac{1}{6\epsilon_0} u_c^2 \int_{-1}^{1} \left[f - 2u_c \left(\frac{x - x_0}{\epsilon_0} \right) \right] \phi(x)\, dx = \lambda\phi, \qquad \phi_x(\pm 1) = 0,$$
$$(A\,4)$$

where we have used (A 3) in (A 2b) to compute η in terms of ϕ. Equation (A 4) may also be obtained by substituting (A 3) into (A 1), where η would then be computed in terms of ϕ by applying the Fredholm alternative to the linearised equation for η. We note that (A 4) is similar to the non-linear eigenvalue problem considered in [9], differing only in the non-local term.

If (A 4) was posed on an infinite domain, $\phi = u_c'$ would be an eigenfunction corresponding to $\lambda = 0$. This is the translation mode. On a finite domain, u_c' fails to satisfy the equation and boundary conditions by exponentially small terms as $\epsilon_0 \to 0$. Thus, we expect that L_{ϵ_0} has an exponentially small eigenvalue and also that ϕ_1 is exponentially close to u_c'. In order for the single-pulse solution to be metastable, however, we require that all other eigenvalues have negative real parts. This is where the non-local term of (A 4) becomes important; as argued in [9] (and references therein), (A 4) without the non-local term has an $O(1)$ positive real eigenvalue that is exponentially close to 5/4. This was confirmed numerically by discretising the local part of L_{ϵ_0} using the second-order difference approximation of the second derivative with grid spacing Δx and computing the eigenvalues of the resulting matrix $\mathscr{A}^{\Delta x}$. To add the contribution of the non-local part of L_{ϵ_0}, we used the trapezoidal rule also with grid spacing Δx to approximate the integral term, constructing the matrix $\mathscr{B}^{\Delta x}$. Computing the eigenvalues of $\mathscr{A}^{\Delta x} + \mathscr{B}^{\Delta x} \equiv \mathscr{C}^{\Delta x}$, we found that, aside from the expected small (positive) eigenvalue, all eigenvalues had negative real parts, regardless of the value of f between 0 and 1. Thus, the small eigenvalue is the principle eigenvalue of (A 4).

The analysis required to estimate the exponentially small eigenvalue λ_1 corresponding to the eigenfunction $\phi_1(x)$ is similar to that performed in [9]. As such, we only show the steps that are specific to this problem. We first give Lagrange's identity for $(v, L_{\epsilon_0}u)$, where $(u, v) = \int_{-1}^{1} uv\, dx$:

$$(v, L_{\epsilon_0}u) = \epsilon^2 (u_x v - v_x u)\big|_{-1}^{1} + (u, L_{\epsilon_0}^* v), \qquad (A\,5a)$$

$$L_{\epsilon_0}^* v \equiv \epsilon_0^2 v_{xx} + (-1 + 2u_c)v + \frac{1}{6\epsilon_0}(f - 2u_c)\int_{-1}^{1} u_c^2 v\, dx. \qquad (A\,5b)$$

We now multiply (A 4) by u_c' and integrate over $-1 < x < 1$, to obtain

$$\lambda_1 (u_c', \phi_1) = -\epsilon_0 u_c'' \phi_1\big|_{-1}^{1} + (\phi_1, L_{\epsilon_0}^* u_c'), \qquad (A\,6)$$

where we have applied (A 5a) to the $(u_c', L_{\epsilon_0}\phi_1)$ term and used $\phi_{1x}(\pm 1) = 0$ to eliminate the boundary terms involving ϕ_{1x}. The terms in (A 6) are the same as those in [9], with the exception being that the non-local part of the adjoint operator $L_{\epsilon_0}^*$ is different. However, the term involving $L_{\epsilon_0}^*$ was shown to be exponentially negligible in [9]; if the same were true in (A 6), we may conclude that the eigenpair λ_1, ϕ_1 is the same as that found in [9] to within exponentially negligible terms. To show this, we first calculate $L_{\epsilon_0}^* u_c'$. Since u_c' is

a solution of the local part of $L^*_{\epsilon_0}$,

$$
\begin{aligned}
L^*_{\epsilon_0} u'_c &= \frac{1}{6\epsilon_0}(f - 2u_c) \int_{-1}^{1} u_c^2 u'_c \, dx \\
&\sim 12(f - 2u_c) \left(e^{-\frac{3}{\epsilon_0}(1-x_0)} - e^{-\frac{3}{\epsilon_0}(1+x_0)} \right),
\end{aligned}
$$

where we have used that

$$
u_c(y) \sim 6e^{\mp y} \quad \text{as} \quad y \to \pm\infty. \tag{A 7}
$$

To estimate $(\phi_1, L^*_{\epsilon_0} u'_c)$, we first recall that ϕ_1 is exponentially close to u'_c, differing only in exponentially small boundary layer terms required to satisfy the no-flux boundary conditions. That is,

$$
\phi_1(x) \sim C_1 u'_c \left(\frac{x - x_0}{\epsilon_0} \right) + e.s.t,
$$

where C_1 is a normalising constant, and *e.s.t* denotes exponentially small terms. Thus, by integrating and applying (A 7), it can be shown that the term

$$
(\phi_1, L^*_{\epsilon_0} u'_c) = 12 \left(e^{-\frac{3}{\epsilon_0}(1-x_0)} - e^{-\frac{3}{\epsilon_0}(1+x_0)} \right) \int_{-1}^{1} (f - 2u_c)\phi_1 \, dx \tag{A 8}
$$

is exponentially smaller than the other two terms in (A 6), leading to the result

$$
\lambda_1 = 60 \left(e^{-\frac{2}{\epsilon_0}(1+x_0)} + e^{-\frac{2}{\epsilon_0}(1-x_0)} \right). \tag{A 9}
$$

As a check, we see from (A 8) that $(\phi_1, L^*_{\epsilon_0} u'_c)$ is exponentially smaller than $O(e^{-3/\epsilon_0})$, while $\lambda_1 = O(e^{-2/\epsilon_0})$. Thus, the term in (A 8) is indeed exponentially negligible. Result (A 9) was confirmed by calculating the eigenvalues of the matrix $\mathscr{C}^{\Delta x}$. Eigenvalues were computed using grid spacings of Δx, $2\Delta x$ and $4\Delta x$ so that Richardson extrapolation could be applied twice to increase the accuracy required for small ϵ. The agreement between (A 9) and the numerical computations is shown in Figure A 1. It should not be surprising that (A 9) is the same expression as that obtained in [9]; the non-linear eigenvalue problem in [9] has the same local terms while the non-local terms in both non-linear eigenvalue problems contribute terms exponentially smaller than the exponential terms in (A 9), and thus in both cases have an exponentially negligible effect on the eigenpair λ_1, ϕ_1.

Since the linearisation around the single-pulse quasi-equilibrium solution yields a principle eigenvalue that is positive but exponentially small as $\epsilon_0 \to 0$, we expect the pulse to evolve on an exponentially slow time scale. As in the calculation of λ_1, the non-local term in (A 4) is insignificant and we thus recover the same result for the motion of the pulse as in [9]:

$$
\frac{dx_0}{d\tau} = 60\epsilon_0 \left(e^{-\frac{2}{\epsilon_0}(1-x_0)} - e^{-\frac{2}{\epsilon_0}(1+x_0)} \right),
$$

or in terms of the original variables t, B and ϵ,

$$
\frac{dx_0}{dt} = 60\epsilon\sqrt{B+1} \left(e^{-\frac{2\sqrt{B+1}}{\epsilon}(1-x_0)} - e^{-\frac{2\sqrt{B+1}}{\epsilon}(1+x_0)} \right). \tag{A 10}
$$

Thus, for $x_0 \neq 0$, the pulse drifts towards the nearest boundary instead of towards

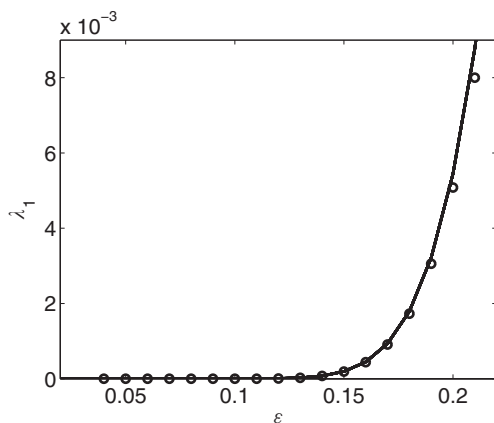FIGURE A 1. Plot λ_1 versus ϵ, where the solid line is the asymptotic estimate (A 9) and the circles are from numerical computations.
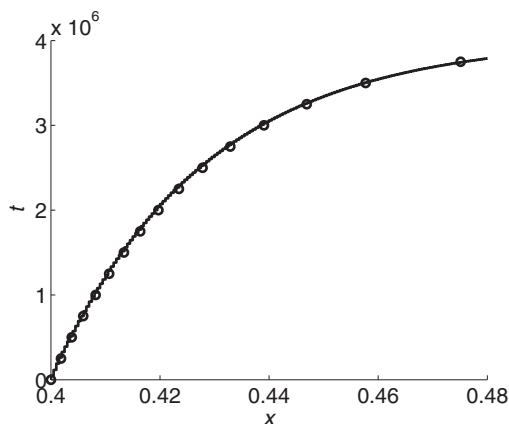

FIGURE A 2. Comparison of asymptotic and numerical results for exponentially slow dynamics of a single pulse starting at $x_0 = 0.4$ for parameters $\epsilon = 0.082$, $A = 2$, $B = 1$, $D = 1$ and $E = 0$. The solid line (circles) represents the numerical (asymptotic) result.

$x = 0$, the latter of which was observed when $E > 0$. The result (A 10) is compared to a numerical solution of (2.1) in Figure A 2, the results of which were verified by grid refinement. We note that the numerical solution is extremely sensitive to the ratio $\sqrt{B+1}/\epsilon$, and for values of the ratio either too large or too small, the match is not as close.

References

[1] CHEN, W. & WARD, M. J. (2011) The stability and dynamics of localized spot patterns in the two-dimensional Gray-Scott model. *SIAM J. Appl. Dyn. Sys.* (to appear).

[2] DE WIT, A., LIMA, D., DEWEL, G. & BORCKMANS, P. (1996) Spatiotemporal dynamics near a codimension-two point. *Phys. Rev. E* **54**, pp. 261–271.

[3] DOELMAN, A., ECKHAUS, W. & KAPER, T. J. (2000) Slowly-modulated two-pulse solutions in the Gray-Scott model : Part I. Asymptotic construction and stability. *SIAM J. Appl. Math.* **61**(3), pp. 1080–1102.

[4] DOELMAN, A., ECKHAUS W. & KAPER, T. J. (2001) Slowly modulated two-pulse solutions in the Gray–Scott model: Part II. Geometric theory, bifurcations, and splitting dynamics. *SIAM J. Appl. Math.* **66**(6), pp. 2036–2062.

[5] DOELMAN, A., GARDNER, R. A. & KAPER, T. J. (1998) Stability analysis of singular patterns in the 1D Gray-Scott model: A matched asymptotic approach. *Physica D* **122**, pp. 1–36.

[6] DOELMAN, A. & KAPER, T. (2003) Semistrong pulse interactions in a class of coupled reaction-diffusion equations. *SIAM J. Appl. Dyn. Syst.* **2**(1), pp. 53–96.

[7] DOELMAN, A., KAPER, T. J. & PROMISLOW, K. (2007) Nonlinear asymptotic stability of the semistrong pulse dynamics in a regularized Gierer–Meinhardt model. *SIAM J. Math. Anal.* **38**(6), pp. 1760–1787.

[8] GIERER, A. & MEINHARDT, H. (1972) A theory of biological pattern Formation. *Kybernetic* **12**, pp. 30–39.

[9] IRON, D. & WARD, M. J. (2000) A metastable spike solution for a nonlocal reaction-diffusion model. *SIAM J. Appl. Math.* **60**(3), pp. 778–802.

[10] IRON, D., WARD, M. J. & WEI, J. (2001) The stability of spike solutions to the one-dimensional Gierer-Meinhardt model. *Physica D* **150**, pp. 25–62.

[11] IRON, D. & WARD, M. J. (2002) The dynamics of multi-spike solutions for the one-dimensional Gierer-Meinhardt Model. *SIAM J. Appl. Math.* **62**(6), pp. 1924–1951.

[12] IRON, D., WEI, J. & WINTER, M. (2004) Stability analysis of turing patterns generated by the Schnakenberg model. *J. Math. Biol.* **49**, pp. 358–390.

[13] KERNER, B. S. & OSIPOV, V. V. (1989) Autosolitons. *Sov. Phys.-Usp.* **32**, pp. 101–138.

[14] KERNER, B. S. & OSIPOV, V. V. (1990) Self-organization in active distributed media: Scenarios for the spontaneous formation and evolution of dissipative structures. *Sov. Phys.-Usp.* **33**, pp. 679–719.

[15] KOLOKOLNIKOV, T., ERNEUX, T. & WEI, J. (2006) Mesa-type patterns in the one-dimensional Brusselator and their stability. *Physica D* **214**, pp. 63–77.

[16] KOLOKOLNIKOV, T., WARD, M. J. & WEI, J. (2005) The existence and stability of spike equilibria in the one-dimensional Gray-Scott model: The low feed rate regime. *Studies in Appl. Math.* **115**(1), pp. 21–71.

[17] KOLOKOLNIKOV, T., WARD, M. J. &WEI, J. (2005) The existence and stability of spike equilibria in the one-dimensional Gray-Scott model: The pulse-splitting regime. *Physica D* **202**(3–4), pp. 258–293.

[18] KOLOKOLNIKOV, T., WARD, M. J. & WEI, J. (2006) Slow translational instabilities of spike patterns in the one-dimensional Gray-Scott model. *Interfaces and Free Boundaries* **8**(2), pp. 185–222.

[19] KOLOKOLNIKOV, T., WARD, M. J. & WEI, J. (2009) Spot self-replication and dynamics for the Schnakenburg model in a two-dimensional domain. *J. Nonlinear Sci.* **19**(1), pp. 1–56.

[20] MURATOV, C. B. & OSIPOV, V. V. (2000) Static spike autosolitons in the Gray-Scott model. *J. Phys. A: Math. Gen.* **33**, pp. 8893–8916.

[21] MURATOV, C. B. & OSIPOV, V. V. (2002) Stability of the static spike autosolitons in the Gray–Scott model. *SIAM J. Appl. Math.* **62**(5), pp. 1463–1487.

[22] NICOLIS, G. & PRIGOGINE, I. (1977) *Self-Organization in Nonequilibrium Systems*, Wiley, New York.

[23] NISHIURA, Y., TERAMOTO, T. & UEDA, K. (2003) Scattering and separators in dissipative systems. *Phys. Rev. E* **67**, 056210.

[24] NISHIURA, Y. & UEYAMA, D. (1999) A skeleton structure of self-replicating dynamics. *Physica D* **130**, pp. 73–104.

[25] PEARSON, J. E. (1993) Complex patterns in a simple system. *Science* **216**, pp. 189–192.

[26] TZOU, J. C., BAYLISS, A., MATKOWSKY, B. J. & VOLPERT, V. A. (2011) Interaction of turing and Hopf modes in the superdiffusive Brusselator model near a codimension two bifurcation point. *Math. Model. Nat. Phenom.* **6**(1), pp. 87–118.

[27] TURING, A. M. (1952) The Chemical Basis of Morphogenesis. *Philos. Trans. R. Soc. London Ser. B* **237**, pp. 3772.

[28] VANAG, V. K. (2004) Waves and patterns in reaction diffusion systems. Belousov-Zhabotinsky reaction in water-in oil microemulsions. *Phys.-Usp.* **47**, pp. 923–941.

[29] WARD, M. J. & WEI, J. (2002) Asymmetric spike patterns for the one-dimensional Gierer-Meinhardt model: Equilibria and stability. *European J. Appl. Math.* **13**(3), pp. 283–320.

[30] WARD, M. J. & WEI, J. (2002) The existence and stability of asymmetric spike patterns for the Schnakenberg model. *Studies in Appl. Math.* **109**, pp. 229–264.

[31] WARD, M. J. & WEI, J. (2008) Hopf bifurcations and oscillatory instabilities of spike solutions for the one-dimensional Gierer-Meinhardt model. *J. Nonlinear Sci.* **13**(2), pp. 209–264.